Activation of TIR signaling is required for pattern-triggered immunity

Hainan Tian[1*], Siyu Chen[1,2*], Zhongshou Wu[1,3*], Kevin Ao[1,3], Hoda Yaghmaiean[1], Tongjun Sun[1], Weijie Huang[1], Fang Xu[1,3,4], Yanjun Zhang[1,3,5], Shucai Wang[6], Xin Li[1,3], and Yuelin Zhang[1]

[1] Department of Botany, University of British Columbia, Vancouver BC V6T 1Z4, Canada

[2] Key Laboratory of Molecular Epigenetics of MOE & Institute of Genetics and Cytology, Northeast Normal University, Changchun, Jilin 130024, China

[3] Michael Smith Laboratories, University of British Columbia, Vancouver BC V6T 1Z4, Canada

[4] The Key Laboratory of Plant Development and Environmental Adaptation Biology, Ministry of Education, School of Life Sciences, Shandong University, Qingdao 266237, China

[5] Institute of Plant Genetics and Developmental Biology, College of Chemistry and Life Sciences, Zhejiang Normal University, Jinhua, Zhejiang 321004, China

[6] College of Life Science, Linyi University, Linyi 276005, China

* These authors contributed equally to the described work.

For correspondence: yuelin.zhang@botany.ubc.ca; xinli@msl.ubc.ca

Abstract

Plant immune responses are mainly activated by two types of receptors. Plasma membrane-localized pattern recognition receptors (PRRs) recognize conserved features of microbes, and intracellular nucleotide-binding leucine rich repeat receptors (NLRs) recognize effector proteins from pathogens. NLRs possessing N-terminal Toll/interleukin-1 receptor (TIR) domains (TNLs) activate two parallel signaling pathways via the EDS1/PAD4/ADR1s and the EDS1/SAG101/NRG1s modules. The relationship between PRR-mediated pattern-triggered immunity (PTI) and TIR signaling is unclear. Here we report that activation of TIR signaling plays a key role in PTI. Blocking TIR signaling by knocking out components of the EDS1/PAD4/ADR1s and EDS1/SAG101/NRG1s modules results in attenuated PTI responses such as reduced salicylic acid (SA) levels and expression of defense genes, and compromised resistance against pathogens. Consistently, PTI is attenuated in transgenic plants that have reduced accumulation of NLRs. Upon treatment with PTI elicitors such as flg22 and nlp20, a large number of genes encoding TNLs or TIR domain-containing proteins are rapidly induced, likely responsible for activating TIR signaling during PTI. In support, overexpression of some of these genes results in activation of defense responses. Overall, our study reveals that TIR signaling activation is an important mechanism for boosting plant defense during PTI.

Introduction

Immune receptors are essential for non-self recognition and defense activation in multicellular organisms [1,2]. Plants use pattern recognition receptors (PRRs), which include transmembrane receptor-like kinases (RLKs) and receptor-like proteins (RLPs), to detect conserved components of microbes collectively known as pathogen-associated molecular patterns (PAMPs), and activate pattern-triggered immunity (PTI) [3]. Unlike RLKs, RLPs do not have a cytoplasmic kinase domain and usually transduce defense signals through adaptor RLKs such as BRI1-ASSOCIATED RECEPTOR KINASE 1 (BAK1) and SUPPRESSOR OF BIR1 1 (SOBIR1) [4]. As an example, RLK FLAGELLIN-SENSITIVE 2 (FLS2) recognizes flg22, a conserved peptide from bacterial flagellin [5,6]. In contrast, *Arabidopsis* RLP23 recognizes a 20-amino-acid motif (nlp20) widely found in most NECROSIS AND ETHYLENE-INDUCING PEPTIDE 1-LIKE PROTEINS (NLPs) of microbes [7,8]. RLP23 constitutively associates with SOBIR1 and binding of nlp20 induces formation of a tripartite complex consisting RLP23, SOBIR1, and BAK1, leading to activation of downstream immune signaling [8].

Activation of PTI typically leads to production of reactive oxygen species (ROS), activation of MITOGEN-ACTIVATED PROTEIN KINASES (MAPKs), increased biosynthesis of the defense hormone salicylic acid (SA) and up-regulation of defense-related genes [9]. Receptor-like cytoplasmic kinases (RLCKs), which have a kinase domain similar to RLKs but lack a transmembrane motif and extracellular ligand-binding domain, play crucial roles in transducing defense signals downstream of PRRs [10].

To promote virulence, microbial pathogens deliver a variety of effector proteins to interfere with PTI and facilitate nutrient acquisition from plants [11]. Recognition of these pathogen effectors by plant immune receptors leads to the activation of effector-triggered immunity (ETI). The majority of intracellular nucleotide-binding leucine-rich repeat proteins (NLRs) serve as sensors for effectors [12]. These sensor

NLRs (sNLRs) with an N-terminal coiled-coil (CC) domain or a Toll/interleukin-1 receptor (TIR) domain are knowns as CNLs and TNLs, respectively. Distinct mechanisms are used by the CC and TIR domains to activate defense signaling. The CC domain of HOPZ-ACTIVATED RESISTANCE 1 (ZAR1) was suggested to form a narrow pore on the plasma membrane to trigger cell death and plant immunity [13]. On the other hand, the TIR domains of many TNLs were shown to possess nicotinamide adenine dinucleotide (NAD+) hydrolase (NADase) activity, which is required for activation of downstream immune responses [14,15]. Intriguingly, two small groups of helper NLRs (hNLRs) in the ADR1 and NRG1 family, which carry an N-terminal RESISTANCE TO POWDERY MILDEW 8 (RPW8)-like CC (CC_R) domain, function downstream of TNLs [16-21]. ADR1s play a critical role in activating SA biosynthesis [22], while NRG1s are required for TNL-induced cell death [17,19]. In addition, three related lipase-like proteins, EDS1 (ENHANCED DISEASE SUSCEPTIBILITY 1)/PAD4 (PHYTOALEXIN DEFICIENT 4)/SAG101 (SENSECENCE-ASSOCIATED GENE 101), also function downstream of TNLs [23]. EDS1 form distinct protein complexes with PAD4 or SAG101. The EDS1/PAD4 complex functions in the same defense pathway as ADR1s, whereas the EDS1/SAG101 complex works together with NRG1 to promote cell death [17,20].

SA plays diverse and critical roles in plant immunity [24,25]. It is required for PTI and ETI in local infection sites, as well as systemic acquired resistance (SAR), which confers protection against secondary infections in distal tissues. In *Arabidopsis*, pathogen-induced SA is mainly synthesized from isochorismate, which is produced from chorismate by ISOCHORISMATE SYNTHASE 1 (ICS1) [26]. PBS3 catalyzes the next step of conjugation of glutamate to isochorismate, and the resulting isochorismate-9-Glu subsequently decomposes to produce SA [27,28]. SAR-DEFICIENT 1 (SARD1) and CALMODULIN BINDING PROTEIN 60g (CBP60g) are two major transcription factors regulating SA biosynthetic genes during pathogen infection [29,30]. Increased *SARD1* expression and SA accumulation are two early events downstream of PRR activation during PTI [9].

NLR homeostasis control is essential for regulating ETI immune output. Ubiquitination plays crucial roles in regulating the NLR protein levels. For example, the turnover of the TNL SNC1 (SUPPRESOR OF *npr1*, CONSTITUTIVE 1) and CNLs RPS2 (RESISTANCE TO *Pseudomonas syringae* 2) and SUMM2 (SUPPRESOR OF *mkk1 mkk2*, 2) is controlled by the Skp, Cullin, F-box (SCF) E3 ligase SCF^{CPR1}[31,32]. Two other E3 ligases MUSE1 (MUTANT, *snc1*-ENHANCING 1) and MUSE2 promote the degradation of several TNLs which pair with SNC1 [33]. Another E3 ligase UBR7 interacts with tobacco TNL N to control its levels [34]. Recently it was also shown that the homeostasis of sensor NLRs is broadly regulated by the redundant E3 ligases SNIPER1 (*snc1*-INFLUENCING PLANT E3 LIGASE REVERSE GENETIC SCREEN) and SNIPER2 [35]. Overexpression of *SNIPER1* leads to globally reduced sNLR levels and attenuated ETI responses.

Immune signaling mediated by PRRs and NLRs has been studied separately in the past; the connection between them is rarely explored. In this study, we tested PAMP-induced responses in *Arabidopsis SNIPER1* overexpression lines and mutants deficient in TNL signaling. Inhibition of NLR accumulation or abolishment of TIR signaling resulted in reduced SA accumulation and compromised PTI, suggesting that activation of TIR signaling plays a crucial role in PTI.

Results

PTI is compromised in *SNIPER1* overexpression lines

Overexpression of *SNIPER1* leads to reduced accumulation of sNLRs and compromised ETI [35]. To test whether PTI is affected in *SNIPER1* overexpression lines, we challenged them with *Pseudomonas syringae pv. tomato* (*Pto*) DC3000 *hrcC*, a bacterial strain unable to secret effectors due to a defect in the type III secretion system. Growth of *Pto* DC3000 *hrcC* was significantly higher in the *SNIPER1* overexpression lines than in wild type (WT) plants (Figure 1A). As no effectors can

be delivered into host cells by *Pto* DC3000 *hrcC*, enhanced growth of this strain in the *SNIPER1* overexpression lines suggests a PTI deficiency. Next, we examined if other PTI responses are affected in these *SNIPER1* overexpression lines. Two defense-related genes *SARD1* and *FMO1* (*FLAVIN-CONTAINING MONOOXYGENASES*) are quickly induced upon infection. The expression levels of *SARD1* and *FMO1* after infection by *Pto* DC3000 *hrcC* were significantly reduced in the *SNIPER1* overexpression lines compared to WT (Figure 1B-C). Furthermore, we measured the SA accumulation induced by *Pto* DC3000 *hrcC*. Both free and glucose-conjugated SA (SAG) levels in the *SNIPER1* overexpression lines were significantly lower than those in the WT plants upon *Pto* DC3000 *hrcC* treatment (Figure 1D, S1A). Taken together, these data suggest that a general reduction of sNLR accumulation due to *SNIPER1* overexpression leads to compromised PTI.

Immune responses induced by nlp20 or flg22 are attenuated in *SNIPER1* overexpression lines

The PTI defects of *SNIPER1* overexpression lines prompted us to test whether *SNIPER1* overexpression affects immune responses induced by the specific PAMP elicitors nlp20 and flg22. To our surprise, the induction of *SARD1* and *FMO1* by nlp20 or flg22 treatment was greatly reduced in the *SNIPER1* overexpression lines compared with WT (Figure 1E and 1F). In addition, SA and SAG levels after nlp20 and flg22 treatment were also significantly lower in the *SNIPER1* overexpression lines than in WT (Figure 1G and 1H, S1B and S1C).

Treatment of nlp20 in local tissues can induce disease resistance in local and distal tissue upon subsequent infection [8]. To determine whether overexpression of *SNIPER1* affects nlp20-induced immunity, we first infiltrated two local leaves with 1 μM nlp20 and sprayed the whole plants with spores of virulent oomycete *Hyaloperonospora arabidopsidis* (*Hpa*) Noco2 one day later. nlp20 treatment induced strong resistance against *Hpa* Noco2 in both the local and distal leaves of WT plants (Figure 1I and 1J). However, the nlp20-induced local as well as systemic resistance to *Hpa* Noco2 were

largely impaired in the *SNIPER1* overexpression lines. Together, these data revealed that a general reduction of sNLRs levels due to *SNIPER1* overexpression results in compromised nlp20 and flg22-induced immune responses.

TNL Signaling components are required for defense against *Pto* DC3000 *hrcC*

As SNIPER1 has been shown to target several TNLs for ubiquitination and degradation [35], we further tested whether activation of TNL signaling is required for PTI. *Pto* DC3000 *hrcC*–induced defense responses were examined in TNL signaling mutants including *eds1-24*, *pad4-1*, *sag101-1*, *adr1 adr1-L1 adr1-L2* (*adr1 triple*) and *nrg1a nrg1b nrg1c* (*nrg1 triple*) mutants. The induction of *SARD1* by *Pto* DC3000 *hrcC* was almost completely blocked in *eds1-24*, *pad4-1* and *adr1 triple* mutant plants, while no change in induction was observed in the *sag101-1* and *nrg1 triple* mutants compared with the WT (Figure S2A). Similarly, the induction of *FMO1* is greatly reduced in *eds1-24*, *pad4-1* and *adr1 triple*, but hardly affected in *sag101-1* and *nrg1 triple* mutant plants (Figure S2B).

We further measured SA accumulation following *Pto* DC3000 *hrcC* infection in these TNL signaling mutants. Both SA and SAG levels in *eds1-24*, *pad4-1* and *adr1 triple* after *Pto* DC3000 *hrcC* treatment were much lower than in the WT (Figure 2A, S2C). This is consistent with the known contributions of EDS1, PAD4 and the ADR1s to pathogen-induced SA biosynthesis. To our surprise, the SA levels after *Pto* DC3000 *hrcC* treatment were also significantly reduced in *sag101-1* and *nrg1 triple* mutant plants, although the reduction was not as dramatic as in *eds1-24*, *pad4-1* and *adr1 triple*. Consistent with the difference in SA levels, growth of *Pto* DC3000 *hrcC* was significantly higher in *sag101-1* and *nrg1 triple* than in WT, and further increased in *eds1-24*, *pad4-1* and *adr1 triple* leaves (Figure 2B). Taken together, PTI responses are significantly attenuated in TNL signaling mutants, indicating a key contribution of TIR signaling to PTI.

flg22-induced immune responses are attenuated in TNL signaling mutants

We then tested PTI responses induced by specific elicitors in the TNL signaling mutants. To determine whether flg22-induced defense responses require TIR signaling, we first compared *SARD1* and *FMO1* induction by flg22 treatment. The expression levels of both *SARD1* and *FMO1* after flg22 treatment were considerably lower in *eds1-24*, *pad4-1* and *adr1 triple* mutant plants (Fig S2D and S2E). In contrast, the expression of *SARD1* was not affected whereas *FMO1* induction was modestly reduced in *sag101-1* and *nrg1 triple*. We also compared the accumulation of SA and SAG after flg22 treatment in WT and the TNL signaling mutants. The SA and SAG levels in *eds1-24*, *pad4-1* and *adr1 triple* plants treated with flg22 were much lower than in the WT (Figure 2C, S2F). Interestingly, the SA levels in *sag101-1* and *nrg1 triple* were also significantly lower compared to the WT, but the difference is not as dramatic as in *eds1-24*, *pad4-1* and *adr1 triple* plants. Consistent with the reduced SA levels, flg22-induced resistance against *Pto* DC3000 was also compromised in *eds1-24*, *pad4-1* and *adr1 triple*, as well as in *sag101-1* and *nrg1 triple* mutant plants, although to a lesser extent (Figure 2D). Taken together, activation of TIR signaling contributes to flg22-induced immune responses.

nlp20-induced immunity is lost in TNL signaling mutants

To determine whether TIR signal components are required for nlp20-induced immune responses, we first examined nlp20-induced *SARD1* and *FMO1* expression in *eds1-24*, *pad4-1*, *sag101-1*, *adr1 triple* and *nrg1 triple* mutants. The induction of *SARD1* and *FMO1* by nlp20 was dramatically reduced in *eds1-24*, *pad4-1* and *adr1 triple* mutant plants, but hardly affected in *sag101-1* and *nrg1 triple* (Figure S2G and S2H). We then measured nlp20-induced SA accumulation in these TNL signaling mutants. The SA and SAG levels after nlp20 treatment were much lower in *eds1-24*, *pad4-1* and *adr1 triple* plants, and moderately lower in *sag101-1* and *nrg1 triple* than in WT (Figure 2E and S2I). Consistent with the reduced SA accumulation, nlp20-induced resistance against *Hpa* Noco2 in both local and distal tissue was attenuated in *sag101-1* and *nrg1 triple* and almost completely blocked in *eds1-24*, *pad4-1* and *adr1 triple* (Figure 2F and S3). Taken together, activation of TIR signaling is required for

nlp20-induced immunity.

Overexpression of genes encoding TIR domain-containing proteins activates defense responses

To understand how TIR signaling is activated during PTI, we analyzed the expression of genes encoding TIR domain-containing proteins (*TIR* genes) in response to nlp20 or flg22 using previously reported RNA-sequencing datasets [36,37]. 26 *TIR* genes were found to be significantly induced 1 h after nlp20 treatment (Table S1). 14 *TIR* genes were considerably induced 6 h after applying nlp20 (Table S2). With flg22 treatment, 46 TIR genes were significantly up-regulated within 30 min (Table S3). These findings suggest that a large number of TIR genes are rapidly induced upon PTI activation.

To test whether up-regulation of *TIR* genes can activate defense responses, we transiently expressed three *TIR* genes induced by both nlp20 and flg22 in *Nicotiana benthamiana*. Among them, *AT4G11170* and *AT3G04220* encode full-length TNLs and *AT2G32140* encodes a protein with only the TIR domain. Overexpression of all three *TIR* genes in *N. benthamiana* leads to activation of cell death around 48 hours after *Agrobacteria* infiltration (Figure 3A). To determine whether overexpression of these three *TIR* genes activates SA biosynthesis, we measured SA levels in samples collected 24 hours and 36 hours after infiltration of the *Agrobacteria* strains, when no macroscopic cell death was visible. In agreement, overexpression of these *TIR* genes in *N. benthamiana* indeed resulted in dramatic increase in SA and SAG levels in *N. benthamiana* (Figure 3B, S4).

Since Ca^{2+} influx is one of the earliest events during PTI, we further examined whether it is involved in activation of the *TIR* genes. To determine whether Ca^{2+} influx is required for nlp20-induced up-regulation of the three *TIR* genes, we pretreated *Arabidopsis* seedling with $GdCl_3$ to block the Ca^{2+} channels prior to nlp20 treatment. Consistent with the RNA-sequencing datasets, treatment with nlp20 or

flg22 alone leads to rapid induction of the three *TIR* genes. However, this induction was completely blocked by $GdCl_3$ (Figure 3C-D), suggesting that activation of Ca^{2+} signaling is required for the induction of *TIR* genes.

nlp20-induced immunity requires the RLCKs PCRK1/2 and PBL19/20

RLCKs PCRK1/2 and PBL19/20 were known to function downstream of PRR receptor kinases such as FLS2 and CERK1 [38-40]. To determine whether they are required for nlp20-induced immunity, we compared growth of *Hpa* Noco2 on WT, *pcrk1/2*, *pcrk1/2 pbl19* and *pcrk1/2 pbl19/20* quadruple mutant plants after treatment with nlp20. nlp20-induced local and systemic resistance against *Hpa* Noco2 was compromised in *pcrk1/2* and *pcrk1/2 pbl19*, and almost completely blocked in *pcrk1/2 pbl19/20* (Figure 4A, S5A). Similarly, nlp20-induced resistance against *Pto* DC3000 was also severely compromised in the *pcrk1/2 pbl19/20* quadruple mutant (Figure S5B). In addition, the increased SA and SAG levels after nlp20 treatment were significantly reduced in *pcrk1/2 pbl19/20* than in the WT (Figure 4B and S5C). Further RT-qPCR analysis showed that nlp20-induced *SARD1* and *FMO1* expression was dramatically reduced in *pcrk1/2 pbl19/20* mutant plants (Figure S5D and S5E). Moreover, induction of the three above-mentioned TIR genes was blocked in *pcrk1/2 pbl19/20* (Figure 4C). Together these data indicate that PCRK1/2 and PBL19/20 are required for nlp20-induced immunity and they act upstream of the early induction of *TIR* genes.

Since SOBIR1 works together with the nlp20 receptor RLP23 in nlp20-activated PTI signal transduction [8], one question is whether PCRK1/2 and PBL19/20 function immediately downstream of SOBIR1. Therefore, we tested whether SOBIR1 directly interacts with PCRK2 and PBL19 using TurboID, a highly efficient proximity labeling method for detecting protein-protein interactions [34,41]. The SOBIR1-HA-TurboID fusion protein was co-expressed with 3×FLAG-tagged PCRK2 or PBL19 in *N. benthamiana*. After biotin treatment, the 3×FLAG-tagged PCRK2 or PBL19 proteins were immunoprecipitated to examine their biotinylation using

Streptavidin-HRP. Both PCRK2 and PBL19 were biotinylated by SOBIR1-HA-TurboID, suggesting that SOBIR1 directly interacts with PCRK2 and PBL19 (Figure 4D). These data agree with the general notion of RLCKs acting immediately downstream of PRRs. We also tested whether SOBIR1 interacts with EDS1/PAD4/ADR1 using TurboID. However, no biotinylation or co-immunoprecipitation of EDS1, PAD4 or ADR1 by SOBIR1-HA-TurboID was observed (Figure S6).

Discussion

PTI and ETI have been traditionally studied as separate defense pathways. Recently it was reported that PTI is required for the activation of NLR-mediated ETI [42,43]. Here, we showed that loss of TIR signaling as well as reduced NLR accumulation results in compromised defense responses activated by nlp20, flg22 and *Pto* DC3000 *hrcC*, indicating that activation of TIR signaling is essential for PTI. While the EDS1/PAD4/ADR1s module plays a predominant role, the EDS1/SAG101/NRG1 module also contributes to flg22, nlp20 and *Pto* DC3000 *hrcC*-induced plant immunity.

SA plays crucial roles in resistance against biotrophic pathogens such as *Hpa* Noco2 and *Pto* DC3000. Activation of PTI leads to rapid increase of SA biosynthesis and elevated SA levels [9]. In the *SNIPER1* overexpression lines, SA levels following nlp20 treatment and *Pto* DC3000 *hrcC* infection are much lower compared to the WT plants. Similarly, nlp20 and *Pto* DC3000 *hrcC*-induced SA accumulation is greatly reduced in *eds1-24*, *pad4-1* and *adr1 triple* mutant plants. In *nrg1 triple* and *sag101-1* mutant plants, SA levels after nlp20 treatment and *Pto* DC3000 *hrcC* infection are also significantly lower than in the wild type. These findings suggest that both the EDS1/PAD4/ADR1s and EDS1/SAG101/NRG1s modules downstream of TIR-type receptors contribute to the up-regulation of SA levels, which plays important roles in defense against pathogens.

In flg22-treated *adr1 triple* mutant plants, SA levels are significantly reduced compared to WT [22]. However, other early PTI responses such as ROS production, MAPK activation and callose deposition induced by flg22 and elf18 are not affected in the *adr1 triple* mutant, suggesting that TIR signaling mediated by ADR1s is not required for the induction of all the very early PTI responses [22]. In flg22-treated *eds1-24*, *pad4-1*, *adr1 triple*, *sag101-1* and *nrg1 triple* mutant plants, flg22-induced resistance against *Pto* DC3000 is significantly reduced but not completely blocked. The loss of TIR signaling is likely compensated by other defense pathways downstream of FLS2, as combining *pad4-1* with the JA biosynthesis mutant *dde2-2*, the ethylene response mutant *ein2-1* (*ethylene insensitive 2-1*) and the SA biosynthesis mutant *sid2-2* (*salicylic acid induction deficient 2-2*) leads to a complete loss of flg22-induced protection against *Pto* DC3000 [44].

In mock-treated *adr1 triple*, *eds1-24* and *pad4-1* mutants, growth of *Pto* DC3000 is much higher than in wild type plants. *adr1 triple*, *eds1-24* and *pad4-1* mutant plants are also more susceptible to *Hpa* Noco2. The general enhanced susceptibility of these mutants to virulent pathogens could be due to compromised PTI caused by loss of the reinforcement of defense responses through activation of TIR signaling.

SARD1 encodes as a master transcription factor regulating the expression of a large number of defense regulators as well as genes involved in SA biosynthesis [45]. Overexpression of *SARD1* leads to increased SA levels and enhanced disease resistance [29] . In WT plants, the expression of *SARD1* is rapidly and strongly induced during PTI. Interestingly, the induction of *SARD1* by nlp20, flg22 and *Pto* DC3000 *hrcC* is dramatically reduced in the *SNIPER1* overexpression lines and mutants deficient in TIR signaling such as *adr1 triple*, *eds1-24* and *pad4-1*, suggesting that the *SARD1* induction during PTI depends on the activation of TIR signaling, which is consistent with the reduced SA levels in the *SNIPER1* overexpression lines and TIR signaling mutants.

A large number of *TIR* genes including *SNC1* and *LAZ5* are rapidly induced after treatment with nlp20 or flg22 (Table S1-S3). Overexpression of *SNC1* and *LAZ5* is known to result in constitutively activated defense responses [46,47] . Similarly, overexpression of the TIR-X protein encoded by *At2g32140* also leads to constitutive activation of EDS1 and PAD4-dependent immune responses [48]. In addition, overexpression of the TIR domains of many TNLs alone is sufficient to activate cell death in *N. benthamiana* [14,15,49]. Recently, many TIR domains have been shown to exhibit NADase activity, likely generating signal molecule(s) activating EDS1-dependent defense responses [14,15]. Induction of the TIR genes during PTI could lead to increased production of these defense signal molecules and activation of downstream TIR signaling pathways and increased SA biosynthesis (Figure 4E). In support of this, transient overexpression of *AT2G32140* and the TNL genes *At4G11170* and *AT3G04220*, which are up-regulated during PTI, resulted in dramatic increase in SA accumulation.

The RLCKs PCRK2 and PBL19 were found to directly interact with SOBIR1. Together with two other closely related RCLKs PCRK1 and PBL20, they are required for nlp20-induced resistance against *Hpa* Noco2. In *pcrk1/2 pbl19/20* quadruple mutant plants, nlp20-induced *SARD1* expression and SA production was blocked. In addition, the induction of several *TIR* genes by nlp20 is also abolished in the *pcrk1/2 pbl19/20* mutant. These findings suggest that PCRK1/2 and PBL19/20 function downstream of the RLP23/SOBIR1 receptor complex to activate the expression of nlp20-responsive *TIR* genes, leading to activation of TIR signaling and SA biosynthesis (Fig 4E). Interestingly, three other RLCKs, PBL30/31/32, were recently reported to be required for nlp20-induced ROS and ethylene production and resistance to *Pto* DC3000 [50]. It is possible that different RLCKs activate different downstream components of the RLP receptor complex, leading to branching of the downstream defense pathways.

In summary, in addition to effector recognition, some TNLs and TIR-X proteins also

play important roles in amplifying PTI responses (Figure 4E). Activation of TIR signaling during PTI is most likely through the induction of *TIR* genes. How the expression of the *TIR* genes is activated is currently unclear. As the induction of several *TIR* genes by nlp20 is blocked by the Ca^{2+} channel blocker $GdCl_3$, elevation in cytosolic Ca^{2+} levels caused by activation of Ca^{2+} channel(s) during PTI may play a crucial role in *TIR* gene induction (Figure 4E). The identities of the transcription factors involved in up-regulation of the *TIR* genes and the mechanism of how Ca^{2+} may affect their activities remains to be determined. Whether PCRK1/2 and PBL19/20 are involved in activation of the Ca^{2+} channel(s) also needs to be determined in the future.

Materials and methods

Plasmid constructs

To generate the CRISPR/Cas9 construct for genome editing of *EDS1A/B* and *PBL20*, genomic sequences of *EDS1* and *PBL20* were subjected to CRISPRscan (http://www.crisprscan.org/?page=sequence) to identify the target sequences. The selected sequences were evaluated with Cas-OFFinder (http://www.rgenome.net/cas-offinder/). The target sequences used for editing *EDS1A/B* was 5'-CTAACCGAGCGCTATCACA(AGG)-3' and 5'-CGGAGAATACATCTCCCTT(TGG)-3', for PBL20 was 5'-CCAAAATCCAGAGGAAATA(TGG)-3' and 5'-CAATAAGTATCCAATTGCTA(TGG)-3'. CRISPR constructs were generated in the *pHEE401E* vector using a previously described CRISPR-Cas9 gene editing system [51].

For coimmunoprecipitation, *PCRK2*, *PBL19* and *ADR1* were amplified by primers PCRK2-Kpn1-F and PCRK2-Spe1-R, PBL19-Kpn1-F and PBL19-BamH1-R, or ADR1-KpnI-F and ADR1-SalI-R, then cloned into pBASTA-35S-3FLAG vector. The *SOBIR1* fragment was cut from pBASTA-35S-SOBIR1-3FLAG plasmid [52], then sub-cloned into pBASTA-35S-2HA-Turbo vector. *EDS1* and *PAD4* were first

amplified by primers EDS1-KpnI-F and EDS1-XbaI-R or PAD4-Kpn1-F and PAD4-BamHI-R, and cloned into pCambia1305-FLAG-ZZ vector [53].

Plant materials and growth conditions

The *pad4-1*, *sag101-1*, *adr1 triple*, *nrg1 triple*, and *pcrk1 pcrk2 (pcrk1/2)* double mutants were previously described [20,22,38,54,55]. The *eds1-24* deletion line was generated by transformation of a *EDS1* CRISPR construct into WT Col-0 plants. Deletion and presence primers were used to detect the presence and homozygosity of the deletion (Supplemental Table 4). The *eds1-24* line is a Cas9 transgene-free line homozygous for a 2636bp deletion, causing truncations of both *EDS1A* (*AT3G48090*) and *EDS1B* (*AT3G48080*).

The *pcrk1 pcrk2 pbl19* (*pcrk1/2 pbl19*) triple mutant was generated by crossing *pcrk1 pcrk2* with *pbl19-2* (Salk_065136C). The *pcrk1 pcrk2 pbl19 pbl20* (*pcrk1/2 pbl19/20*) quadruple mutants were generated by transforming the CRISPR/Cas9 construct targeting *PBL20* into the *pcrk1 pcrk2 pbl19* triple mutant background. Both *pcrk1 pcrk2 pbl19 pbl20* #33 and #47 lines carry a large 1.5 kb deletion in *PBL20*. All the mutants are in the Col-0 background. The transgenic OX-*SNIPER1* #4, OX-*SNIPER1* #5 lines were generated previously in a reverse genetics screen for plant immunity related E3 ligases [20].

Plants were grown in growth rooms with a temperature of 23°C under long day (16h light/8h dark) or short day (12h light/12h dark) condition at approximately 100 μmol m^{-2} s^{-1} light intensity. For *Agrobacterium* mediated transformation, the *Arabidopsis* seeds were directly sown on soil and grown for around 5 weeks prior to floral-dip transformation. For RNA isolation, the *Arabidopsis* seeds were sterilized in 15% (v/v) bleach and germinated on plates with ½ Murashige and Skoog (MS) with vitamins (PlantMedia) and 1% (w/v) sucrose.

RNA extraction and gene expression

For analyzing nlp20/flg22 induced gene expression, total RNA was extracted from 12-day-old plate-grown seedlings 4 hours after spraying 1 μM flg22 or 1μMnlp20. To test pathogen-induced gene expression, leaves of four-week-old plants grown under short day conditions were infiltrated with *Pto* DC3000 *hrcC* at a dose of OD_{600}=0.05 and collected after 12hours. RNA was extracted using the EZ-10 Spin Column Plant RNA Mini-Preps Kit (Bio Basic, Canada) according to the manufacturer's instructions. 1 μg RNA was used for cDNA synthesis by Oligo(dT)-primed reverse transcription using the OneScript Reverse Transcriptase kit (ABM, Canada). Real-time quantitative PCR was performed to analyze the gene expression levels, using the SYBR Premix Ex Taq II kit (TAKARA). The primers used for qPCR were reported previously [45]. *ACTIN1* was used as an internal control. For nlp20-induced *TIR* gene expression analysis, 10-day-old seedlings grown on ½ MS medium were transferred to ½ MS liquid medium. After 24-hour recovery, nlp20 was supplied to a 1 μM final concentration. Two to three individual plants treated with nlp20 were harvested 1 hour later as one sample. *ACTIN7* was used as an internal control. The primers used are listed in Supplemental Table 4.

Measurement of Salicylic acid

The procedure for SA extraction and measurement was reported previously[56]. In brief, for each sample, about 100mg leaf tissue was collected from 25-d-old soil-grown plants and grounded in liquid nitrogen. Each genotype contains four biological replicates, with each sample collected from three different plants. For every sample, 0.6 ml of 90% methanol was added, and the sample was vortexed 20s and sonicated for 20 min to release SA. Samples were then centrifuged at 12000×g for 10 min. The supernatant was collected and another 0.5 ml of 100% methanol was added to the pellet for a second round of extraction. The supernatant from both extractions were combined and dried by vacuum. Then 0.5 ml 5% (w/v) trichloroacetic acid was added to the dry samples, vortexed and sonicated for 5 min, and then centrifuged at 12000×g for 15 min. The supernatant was collected and then extracted three times with 0.5 ml extraction buffer (ethylacetate acid/ cyclopentane/ isoporopanal: 100/99/1 by volume).

Each time, after centrifugation at 12,000×g for 10 min, the organic phase was collected and combined to a new tube and dried by vacuum afterwards. The final dried sample was resuspended in 200 µl mobile phase (0.2M KAc, 0.5mM EDTA PH=5) by vortexing and sonicating for 5 min. After spinning at 12,000×g for 5 min, the supernatant was kept and measured by high-performance liquid chromatography (HPLC) to measure the amount of SA as compared with a standard.

Pathogen infection assay

For *Pto* DC3000 *hrcC* bacterial growth assays, two fully extended leaves of four-week-old plants grown under short-day conditions were infiltrated with *Pto* DC3000 *hrcC* at a dose of OD_{600} =0.002. Samples were collected at 0 day and 3 days after infiltration. One sample contained two leaf discs from a single plant, and a single leaf disc was collected from each infected leaf. The samples were ground, diluted in 10 mM $MgCl_2$, and plated on Lysogeny broth (LB) agar plates containing 25 µg ml^{-1} Rifampicin. After incubation at 28℃ for 36 h, colonies were counted from selected dilutions and the colony numbers were used to calculate the colony forming units. For flg22/nlp20-induced pathogen resistance, leaves of four-week-old plants were infiltrated with 1 µM flg22/nlp20 or H_2O as control. After 24h, the same treated leaves were infiltrated with *Pto* DC3000 at a dose of OD_{600}=0.001. After 3 days, samples were collected and analyzed as above.

To analyze nlp20-induced SAR, leaves of three-week-old plants were first infiltrated with 1 µM nlp20. After 24 h, plants were sprayed with *Hpa* Noco2 spore suspension at a concentration of 50,000 per ml water. Then plants were covered with a clean dome and grown at 18℃ under short-day conditions in a growth chamber. After 7 days, the *Hpa* Noco2 sporulation was scored as previously described [57].

TurboID-based proximity labeling in *N. benthamiana*, immunoprecipitation and western blot analysis

TurboID-based proximity labeling assay was performed as described previously [20]. In brief, *N. benthamiana* leaves were infiltrated with *Agrobacterium* containing *HA-TurboID* and *ZZ-TEV-FLAG* or *3xFLAG* tagged constructs. At 48 hpi, biotin was infiltrated, and the plants were incubated at room temperature for 2 hours to allow biotin labeling. About 2.0 g *N. benthamiana* leaves expressing the indicated proteins were harvested at 50 hpi and ground into powder with liquid nitrogen. Extraction buffer containing 25 mM Tris-HCl pH 7.5, 150 mM NaCl, 1mM EDTA, 0.3% Nonidet P-40, 10% Glycerol, 1 mM PMSF, 1× Protease Inhibitor Cocktail (Roche; Cat. #11873580001), and 10 mM DTT. The FLAG-tagged PCRK2 and PBL19 proteins were immunoprecipitated using 15 µl M2 beads (Sigma; Cat. #A2220). Biotinylation was detected with Streptavidin-HRP (Abcam Cat. # ab7403). The anti-HA antibody was from Roche (Cat. #11867423001). The anti-FLAG antibody was from Sigma (Cat. #F1804).

Bioinformatic analysis for TIR-containing gene induction

TIR genes induced 30 minutes after flg22 treatment were subset from previously published data [58]. For nlp20-induced genes, previously published raw RNA-seq reads were retrieved (GSE133053) [36]. BBDuk (https://sourceforge.net/projects/bbmap/) was used to trim adapters. A decoy-aware reference transcriptome was generated using a high-quality *Arabidopsis* reference transcriptome, AtRTDv2_QUASI_19April2016.fa [59], and an *Arabidopsis* whole genome sequence (Ensembl Plants version 47) as a decoy. Salmon v1.2.1 [60]was used to build an index and quantify transcript expression against the reference transcriptome using default parameters. Transcript-level expression (TPM values) were imported to R and summarized to gene-level expression using tximport v1.16.1 [61]. DESeq2 v1.28.1 [62] was used to determine differentially-expressed genes (padj < 0.1). Genes were annotated using biomaRt v2.44.1 [63], and genes containing TIR domains (IPR035897, IPR000157, IPR041340, IPR017279) were subset.

Author Contributions

HT, SC and ZW carried out the majority of the experiments. KA generated *eds1-24*, and extracted the up-regulated *TIR* genes from RNA-Sequencing datasets. WH and YZ helped with HPLC SA analysis. FX made the FLAG-ZZ tagged EDS1 and PAD4 constructs. HY and TS generated the combined RLCK mutants. YZ, SW and XL wrote the manuscript with contributions of all authors.

Competing financial interests

The authors declare no competing financial interests.

Acknowledgements

We would like to thank Drs. Jane Parker, Jeff Dangl and Jian-Min Zhou for sharing mutant seeds and pathogen strains. Mr. Lei Tian is thanked for help with the HPLC analysis. Dr. Thorsten Nuernberger is thanked for insightful discussions. This study was financially supported by grants to XL and YZ from the Natural Sciences and Engineering Research Council (NSERC) Discovery program of Canada, NSERC-CREATE-PRoTECT, and the Canadian Foundation for Innovation (CFI), grant to YZ from National Natural Science Fundation of China (31828008), scholarships to HT, SC, WH and ZW from the Chinese Scholarship Council, and scholarships to KA from the Alexander Graham Bell Canada Graduate Scholarship Doctoral Program, and the University of British Columbia Four-year fellowship program.

Figure legends:

Figure 1. Overexpression of *SNIPER1* leads to attenuation of *Pto* DC3000 *hrcC*, flg22 and nlp20-induced immunity.

(A) Growth of *Pto* DC3000 *hrcC* in wild type (WT) Col-0 and two independent *SNIPER1* overexpression (OX-*SNIPER1*) lines. Leaf discs were collected 0 days (Day 0) or 3 days (Day 3) after bacterial infiltration (OD_{600}=0.002). Error bars represent standard deviation (SD) from four biological replicates. The growth of *Pto* DC3000 *hrcC* in different genotypes on Day 3 was compared using two-way ANOVA test, and different letters indicate genotypes with statistical differences ($p < 0.05$; n = 4). The experiment was repeated twice with similar results.

(B, C) Relative expression levels of *SARD1* (B) and *FMO1* (C) in WT and *OX-SNIPER1* plants upon *Pto* DC3000 *hrcC* infection. Total RNA was isolated from leaf tissues of 25-d-old soil-grown plants 12 hours after infiltration with *Pto* DC3000 *hrcC* (OD_{600}=0.05) or 10 mM $MgCl_2$ (Mock). qPCR was used to examine the genes expression levels. *ACT1* was used for normalization, and the expression of each gene in mock-treated WT plants was set as 1. Error bars represent SD from three different biological replicates. Different letters indicate genotypes with statistical differences ($p < 0.05$, one-way ANOVA test; n=3). The experiment was repeated twice with similar results.

(D) Free salicylic acid (SA) levels in four-week-old WT and OX-*SNIPER1* plants 12 hours after treatment with 10 mM $MgCl_2$ (mock) or *Pto* DC3000 *hrcC*. Different letters indicate genotypes with statistical differences ($p < 0.05$, one-way ANOVA test; n=3). The experiment was repeated three times with similar results.

(E, F) Relative expression levels of *SARD1* and *FMO1* in WT and *OX-SNIPER1* plants upon 1 μM nlp20 (E) or 1 μM flg22 (F) treatment. Total RNA was isolated from 12-d-old plate-grown seedlings 4 hours after spraying with 1 μM nlp20 (A) or 1 μM flg22 (B). *ACT1* was used for normalization, and the expression of each gene in the H_2O (mock)-treated WT plants was set as 1. Error bars represent SD from three

different biological replicates. Different letters indicate genotypes with statistical differences ($p < 0.05$, one-way ANOVA test; n=3). The experiment was repeated twice with similar results.

(G, H) Levels of free SA in WT and OX-*SNIPER1* plants upon 1 μM nlp20 (G) or 1 μM flg22 (H) treatment. 25-d-old soil-grown plants samples were collected 24 hours after treatment with nlp20, and 9 hours after treatment with flg22. H_2O served as mock treatment. Different letters indicate genotypes with statistical differences ($p < 0.05$, one-way ANOVA test; n=3). The experiment was repeated three times with similar results.

(I) Growth of *Hpa* Noco2 on the local leaves of WT and *OX-SNIPER1* plants with or without nlp20 treatment. Three-week-old plants were pretreated with water (H_2O) or 1 μM nlp20 and sprayed with *Hpa* Noco2 spores (50,000 spores/ml) 24 hours later. Infection was scored at 7 days post inoculation (dpi) by counting the number of conidiophores per infected leaf. A total of 15 plants were scored for each treatment. Disease rating scores are as follows: 0, no conidiophores on the infected leaves; 1, no more than 5 conidiophores on one infected leaf; 2, 6 to 20 conidiophores on one infected leaf; 3, 20 or more conidiophores on one infected leaf; 4, 5 or more conidiophores on two infected leaves; 5, 20 or more conidiophores on two infected leaves. This experiment was repeated twice with similar results.

(J) Growth of *Hpa* Noco2 on the distal leaves of WT and OX-*SNIPER1* plants in an SAR assay. 15 plants were used for each treatment. Disease symptoms were scored 7 dpi by counting the number of conidiophores on the distal leaves. Disease ratings: 0, no conidiophores on plants; 1, one leaf is infected with no more than five conidiophores; 2, one leaf is infected with more than five conidiophores; 3, two leaves are infected but with no more than five conidiophores on each infected leaf; 4, two leaves are infected with more than five conidiophores on each infected leaf; 5, more than two leaves are infected with more than five conidiophores.

The experiment was repeated twice with similar results.

Figure 2. Contributions of TIR signaling components to *Pto* DC3000 *hrcC*, flg22

and nlp20-induced immunity.

(A) Levels of free SA in four-week-old soil-grown WT, *eds1-24*, *pad4-1*, *sag101-1*, *adr1 triple* and *nrg1 triple* mutants 12 hours after treatment with 10 mM $MgCl_2$ or *Pto* DC3000 *hrcC* (OD_{600}=0.05) for 12 hours. Different letters indicate genotypes with statistical differences ($p < 0.05$, one-way ANOVA test; n=3). The experiment was repeated three times with similar results.

(B) Growth of *Pto*DC3000 *hrcC* in 25-day-old soil-grown plants of the indicated genotypes. Leaf discs were collected 0 days (Day 0) or 3 days (Day 3) after *Pto* DC3000 *hrcC* (OD_{600}=0.002) infiltration. Error bars represent SD from four biological replicates. The growth of *Pto* DC3000 *hrcC* in different genotypes was compared using two-way ANOVA test, and different letters indicate genotypes with statistical differences ($p < 0.05$, $n = 4$). The experiment was repeated twice with similar results.

(C) Levels of free SA in four-week-old soil-grown plants of the indicated genotypes after treatment with water or 1 μM flg22 for 9 hours. Different letters indicate genotypes with statistical differences ($p < 0.05$, one-way ANOVA test; n=3). The experiment was repeated three times with similar results.

(D) Growth of *Pto* DC3000 in the leaves of four-week-old WT, *eds1-24*, *pad4-1*, *sag101-1*, *adr1 triple* and *nrg1 triple* mutant plants after treatment with water or 1 μM flg22. 24 hours later, the same treated leaves were infiltrated with *Pto* DC3000. Samples were taken 3 days after *Pto* DC3000 inoculation. Error bars represent SD from six biological replicates. The flg22-induced protection among different genotypes was compared using two-way ANOVA test, and different letters indicate genotypes with statistical differences ($p < 0.05$, $n= 6$). The experiment was repeated twice with similar results.

(E) Levels of free SA in four-week-old soil-grown plants of the indicated genotypes after treatment with water (mock) or 1 μM nlp20 for 24h. Different letters indicate genotypes with statistical differences ($p < 0.05$, one-way ANOVA test; n=3). The experiment was repeated three times with similar results.

(F) Growth of *Hpa* Noco2 on the local leaves of the indicated plants. Three-week-old

636 soil-grown plants were pretreated with water or 1 μM nlp20 and sprayed with *Hpa*
637 Noco2 spores (50,000 spores/ml) 24 hours later. Disease ratings are as described in
638 Fig 1. The experiment was repeated twice with similar results.
639
640 **Figure 3. Overexpression of *TIR* genes activates SA biosynthesis in *N.***
641 ***benthamiana.***
642 (A) Hypersensitive response (HR) in the *N. benthamiana* leaves expressing the TIR
643 genes *At4g11170*, *At3g04220* or *At2g32140* through *Agrobacterium tumefaciens*
644 GV3101 (OD_{600}=0.4) infiltration. Photographs were taken 3 days after *Agrobacterium*
645 infiltration. The empty vector (EV) treatment serves as control; 1, *At4g11170*; 2,
646 *At3g04220*; 3, *At2g32140*.
647 (B) Levels of free SA in *N. benthamiana* leaves after infiltration of *Agrobacterium*
648 (OD_{600}=0.4) carrying the *TIR* genes from (A). Samples were collected 24 and 36
649 hours post infiltration, before HR was visible. Error bars represent SD from three
650 biological replicates. Different letters indicate different time course with statistical
651 differences ($p < 0.05$, one-way ANOVA test; n=3).
652 (C, D) Induction of the indicated *TIR* genes by nlp20 (C) or flg22 (D). Ten-day--old
653 plate-grown WT plants were transplanted to water 1 day before for recovery and then
654 pretreated with water (Mock) or 100 μM $GdCl_3$ for 1 hour. Samples were collected 1
655 hour after supplying with 1 μM nlp20 or 1 μM flg22. qPCR was used to examine the
656 genes expression level. *ACT7* was used for normalization. Error bars represent SD
657 from three different biological replicates. Different letters indicate different treatment
658 with statistical differences ($p < 0.05$, one-way ANOVA test; n=3)
659 All the experiments were repeated twice with similar results.
660
661 **Figure 4. PCRK1/2 and PBL19/20 are required for nlp20-induced immunity.**
662 (A) Growth of *Hpa* Noco2 on the distal leaves of WT, *pcrk1/2*, *pcrk1/2 pbl19*, p*crk1/2*
663 *pbl19/20* #33 and *pcrk1/2 pbl19/20* #47 quadruple mutant plants. 21-d-old soil-grown
664 plants were treated with 1 μM nlp20 and sprayed *Hpa* Noco2 spores (50,000
665 spores/ml) 24 hours later. The detail method was described in Fig 2F.

(B) Levels of free SA in four-week-old soil-grown plants of the indicated genotypes treated with water or 1 μM nlp20. Samples were collected 24 hours post elicitor treatment. Different letters indicate genotypes with statistical differences ($p < 0.05$, one-way ANOVA test; n=3).

(C) The induction of *At4g11170*, *At3g04220* and *At2g32140* (*TIR* genes) in the indicated genotypes. Total RNA was isolated from seedlings of 10-d-old plate-grown plants 1 h after treatment with 1 μM nlp20. *ACT7* was used for normalization, and the expression of each gene in mock-treated WT was set as 1. Error bars represent SD from three different biological replicates. Different letters indicate genotypes with statistical differences ($p < 0.05$, one-way ANOVA test; n=3).

(D) Immunoprecipitation and biotinylation of *PCRK2*/*PBL19-3FLAG* by *SOBIR1-HATurboID* in *N. benthamiana*. *Agrobacterium* carrying the indicated constructs were infiltrated into *N. benthamiana* leaves for protein expression. Immunoprecipitation was carried out with anti-FLAG beads. The 3FLAG-tagged proteins were detected using an anti-FLAG antibody. The biotinylated proteins were detected using HRP-Streptavidin. The experiments in (A-D) were repeated twice with similar results.

(E) A working model for the contribution of TIR signaling in PTI. Upon perception of pathogen elicitors such as flg22 and nlp20, PRRs activate early immune responses such as ROS production, MAPK activation and Ca^{2+} influx through RLCKs. Elevated cytosolic Ca^{2+} levels induce the expression of a large number of *TIR* genes, leading to activation of downstream defense pathways through the EDS1/PAD4/ADR1s and EDS1/SAG101/NRG1s signaling modules. Activation of TIR signaling further induces downstream defense gene expression, resulting in increased SA biosynthesis and enhanced resistance to pathogens. In parallel, activation of MAPKs promotes the biosynthesis of ethylene.

694 **Supplementary tables:**

695

696 **Table S1: TIR genes induced by flg22 30 min after treatment.**

697

698 **Table S2: TIR genes induced by nlp20 1h after treatment.**

699

700 **Table S3: TIR genes induced by nlp20 6h after treatment.**

701

702 **Table S4: Sequence of primers used in this study.**

703

704

705

706 **Supplementary figure legends:**

707

708 **Figure S1. Levels of glucose-conjugated SA (SAG) in WT and OX-*SNIPER1***
709 **plants.**
710 (A) SAG levels in four-week-old soil-grown WT and OX-*SNIPER1* plants treated
711 with 10 mM $MgCl_2$ (mock) or *Pto* DC3000 *hrcC*.
712 (B, C) SAG levels in 25-d-old plants WT and OX-*SNIPER1* plants treated with H_2O
713 (mock), 1 µM nlp20 (B) or 1 µM flg22 (C).
714 Samples were collected for SAG measurement 24 hr after 1µM nlp20, or 9 hr after
715 1µM flg22 treatment. Different letters indicate genotypes with statistical differences
716 ($p < 0.05$, one-way ANOVA test; n=3). All the experiments were repeated three times
717 with similar results.
718

719 **Figure S2. Induction of *SARD1* and *FMO1* gene expression and SAG production**
720 **in TIR signaling mutants upon *Pto* DC3000 *hrcC*, flg22 or nlp20 treatment.**
721 (A, B) Relative expression levels of *SARD1* (A) and *FMO1* (B) in WT, *eds1-24*,
722 *pad4-1*, *sag101-1*, *adr1 adr-L1 adr-L2* (*adr1 triple*) and *nrg1a nrg1b nrg1c* (*nrg1*
723 *triple*) mutant plants after treatment with *Pto* DC3000 *hrcC* (OD_{600} = 0.05) for 12
724 hours. Error bars represent SD from three different biological replicates. Different
725 letters indicate genotypes with statistical differences ($p < 0.05$, one-way ANOVA test;
726 n=3).
727 (C, F, I) Four-week-old soil-grown plants of the indicated genotypes were treated with
728 *Pto* DC3000 *hrcC* (OD_{600}=0.05) (D), 1 µM flg22 (F) or 1 µM nlp20 (I). Samples were
729 collected for SAG measurement 12 hr after inoculation of *Pto* DC3000 *hrcC*, 24 hr
730 after treatment with 1 µM nlp20, or 9 hr after treatment with 1 µM flg22. Different
731 letters indicate genotypes with statistical differences ($p < 0.05$, one-way ANOVA test;
732 n=3). The experiment was repeated three times with similar results.
733 (D, E) Relative expression levels of *SARD1* (D) and *FMO1* (E) in the indicated
734 genotypes upon flg22 treatment. Total RNA was isolated from 12-d-old plate-grown
735 seedlings 4 h after spraying with 1 µM flg22. Different letters indicate genotypes with

736 statistical differences ($p < 0.05$, one-way ANOVA test; n=3).
737 (G, H) Relative expression levels of *SARD1* (G) and *FMO1* (H) in the indicated
738 genotypes upon nlp20 treatment. Total RNA was isolated from 12-d-old plate-grown
739 seedlings 4 h after spraying with 1 μM nlp20. Different letters indicate genotypes with
740 statistical differences ($p < 0.05$, one-way ANOVA test; n=3).
741 For gene expression analysis in (A, B, D, E, G, H), the expression of each gene in the
742 mock-treated WT plants was set as 1. All gene expression analyses were repeated
743 twice with similar results.
744
745 **Figure S3. Growth of *Hpa* Noco2 on the distal leaves of TIR signaling mutants.**
746 **mutants.**
747 Three-week-old soil-grown plants were pretreated with water or 1 μM nlp20 and
748 sprayed with *Hpa* Noco2 spores (50,000 spores/ml) 24 hours later. Disease ratings are
749 as described in Fig 1. The experiment was repeated twice with similar results.
750
751 **Figure S4. Levels of glucose-conjugated SA (SAG) in *N. benthamiana* leaves after**
752 **infiltration of *Agrobacterium* carrying the *TIR* genes.**
753 Samples were collected 24 and 36 hours post infiltration of the bacteria (OD_{600}=0.4)
754 before HR was visible. Different letters indicate statistical differences ($p < 0.05$,
755 one-way ANOVA test; n=3) compared with the empty vector control. The experiment
756 was repeated twice with similar results.
757
758 **Figure S5. nlp20-induced immune responses are compromised in *pcrk1/2***
759 ***pbl19/20* quadruple mutant plants.**
760 (A) Growth of *Hpa* Noco2 on the local leaves of WT, *pcrk1/2*, *pcrk1/2 pbl19*, p*crk1/2*
761 *pbl19/20* #33 and *pcrk1/2 pbl19/20* #47 quadruple mutant plants after 1 μM nlp20
762 treatment. Infection was scored 7 dpi by counting the number of conidiophores per
763 infected leaf. Detailed methodology was described in Fig 2E.
764 (B) Growth of *Pto* DC3000 in the leaves of four-week-old WT, *pcrk1/2 pbl19/20* #33
765 and *pcrk1/2 pbl19/20* #47 quadruple mutant plants pre-treated with water or 1 μM

nlp20. 24 hours post elicitor treatment, the treated leaves were infiltrated with *Pto* DC3000 (OD_{600}=0.001). Samples were taken 3 days after *Pto* DC3000 inoculation. Error bars represent SD from six biological replicates. The nlp20-induced protection among different genotypes was compared using two-way ANOVA test, and different letters indicate genotypes with statistical differences ($p < 0.05$, n= 6).

(C) Levels of SAG in four-week-old soil-grown plants of the indicated genotypes treated with water or 1 μM nlp20. Samples were collected 24 hours post elicitor treatment. Different letters indicate statistical differences ($p < 0.05$, one-way ANOVA test; n=3)

(D, E) Relative expression levels of *SARD1* (D) and *FMO1* (E) in the indicated genotypes. Total RNA extracted from 12-d-old plate-grown plants treated with 1 μM nlp20 for 4h. *ACT1* was used for normalization, and the expression of each gene in mock-treated WT was set as 1. Error bars represent SD from three different biological replicates. Different letters indicate genotypes with statistical differences ($p < 0.05$, one-way ANOVA test; n=3).

All the experiments were repeated twice with similar results.

Figure S6. Analysis of interactions between SOBIR1 and EDS1/PAD4/ADR1 by TurboID and co-immunoprecipitation analysis.

Agrobacterium carrying the indicated constructs were infiltrated into *N. benthamiana* leaves for protein expression. Immunoprecipitation of EDS1-FLAG-ZZ, PAD4-FLAG-ZZ or ADR1-3FLAG was carried out with anti-FLAG beads. The 3FLAG-tagged and HATurboID fusion proteins were detected by western blot using an anti-FLAG or anti-HA antibody by western blot. The biotinylated proteins were detected by western blot using HRP-Streptavidin. Molecular mass marker in kiloDaltons is indicated on the left. The experiment was repeated twice with similar results.

References:

1 Zhou, J. M. & Zhang, Y. Plant Immunity: Danger Perception and Signaling. *Cell* **181**, 978-989, doi:10.1016/j.cell.2020.04.028 (2020).

2 Jones, J. D. & Dangl, J. L. The plant immune system. *Nature* **444**, 323-329 (2006).

3 Monaghan, J. & Zipfel, C. Plant pattern recognition receptor complexes at the plasma membrane. *Curr Opin Plant Biol* **15**, 349-357, doi:10.1016/j.pbi.2012.05.006 (2012).

4 Liebrand, T. W., van den Burg, H. A. & Joosten, M. H. Two for all: receptor-associated kinases SOBIR1 and BAK1. *Trends Plant Sci* **19**, 123-132, doi:10.1016/j.tplants.2013.10.003 (2014).

5 Gomez-Gomez, L. & Boller, T. FLS2: an LRR receptor-like kinase involved in the perception of the bacterial elicitor flagellin in Arabidopsis. *Mol Cell* **5**, 1003-1011 (2000).

6 Felix, G., Duran, J. D., Volko, S. & Boller, T. Plants have a sensitive perception system for the most conserved domain of bacterial flagellin. *The Plant Journal* **18**, 265-276 (1999).

7 Böhm, H. *et al.* A conserved peptide pattern from a widespread microbial virulence factor triggers pattern-induced immunity in Arabidopsis. *PLoS Pathog* **10**, e1004491 (2014).

8 Albert, I. *et al.* An RLP23–SOBIR1–BAK1 complex mediates NLP-triggered immunity. *Nature Plants* **1**, 1-9 (2015).

9 Peng, Y., Wersch, R. v. & Zhang, Y. Convergent and divergent signaling in PAMP-triggered immunity and Effector-triggered immunity. *Molecular Plant-Microbe Interactions* (2017).

10 Liang, X. & Zhou, J.-M. Receptor-like cytoplasmic kinases: central players in plant receptor kinase–mediated signaling. *Annual review of plant biology* **69**, 267-299 (2018).

11 Toruño, T. Y., Stergiopoulos, I. & Coaker, G. Plant-pathogen effectors: cellular probes interfering with plant defenses in spatial and temporal manners. *Annual review of phytopathology* **54**, 419-441 (2016).

12 Li, X., Kapos, P. & Zhang, Y. NLRs in plants. *Current opinion in immunology* **32**, 114-121, doi:10.1016/j.coi.2015.01.014 (2015).

13 Wang, J. *et al.* Reconstitution and structure of a plant NLR resistosome conferring immunity. *Science* **364** (2019).

14 Wan, L. *et al.* TIR domains of plant immune receptors are NAD+-cleaving enzymes that promote cell death. *Science* **365**, 799-803 (2019).

15 Horsefield, S. *et al.* NAD+ cleavage activity by animal and plant TIR domains in cell death pathways. *Science* **365**, 793-799 (2019).

16 Peart, J. R., Mestre, P., Lu, R., Malcuit, I. & Baulcombe, D. C. NRG1, a CC-NB-LRR protein, together with N, a TIR-NB-LRR protein, mediates resistance against tobacco mosaic virus. *Curr Biol* **15**, 968-973, doi:10.1016/j.cub.2005.04.053 (2005).

17 Qi, T. *et al.* NRG1 functions downstream of EDS1 to regulate TIR-NLR-mediated plant immunity in Nicotiana benthamiana. *Proceedings of the National Academy of Sciences* **115**, E10979-E10987 (2018).

18 Lapin, D. *et al.* A coevolved EDS1-SAG101-NRG1 module mediates cell death signaling by TIR-domain immune receptors. *The Plant cell* **31**, 2430-2455 (2019).

19 Castel, B. *et al.* Diverse NLR immune receptors activate defence via the RPW 8 - NLR NRG 1. *New Phytologist* **222**, 966-980 (2019).

20 Wu, Z. *et al.* Differential regulation of TNL - mediated immune signaling by redundant helper

CNLs. *New Phytologist* **222**, 938-953 (2019).

21 Dong, O. X. *et al.* TNL‐mediated immunity in Arabidopsis requires complex regulation of the redundant ADR1 gene family. *New Phytologist* (2016).

22 Bonardi, V. *et al.* Expanded functions for a family of plant intracellular immune receptors beyond specific recognition of pathogen effectors. *Proc Natl Acad Sci U S A* **108**, 16463-16468, doi:10.1073/pnas.1113726108 (2011).

23 Wiermer, M., Feys, B. J. & Parker, J. E. Plant immunity: the EDS1 regulatory node. *Curr Opin Plant Biol* **8**, 383-389, doi:10.1016/j.pbi.2005.05.010 (2005).

24 Liu, Y. *et al.* Diverse roles of the salicylic acid receptors NPR1 and NPR3/NPR4 in plant immunity. *The Plant cell* **32**, 4002-4016 (2020).

25 Zhang, Y. & Li, X. Salicylic acid: biosynthesis, perception, and contributions to plant immunity. *Curr Opin Plant Biol* **50**, 29-36, doi:10.1016/j.pbi.2019.02.004 (2019).

26 Wildermuth, M. C., Dewdney, J., Wu, G. & Ausubel, F. M. Isochorismate synthase is required to synthesize salicylic acid for plant defence. *Nature* **414**, 562-565 (2001).

27 Torrens-Spence, M. P. *et al.* PBS3 and EPS1 complete salicylic acid biosynthesis from isochorismate in Arabidopsis. *Molecular plant* **12**, 1577-1586 (2019).

28 Rekhter, D. *et al.* Isochorismate-derived biosynthesis of the plant stress hormone salicylic acid. *Science* **365**, 498-502, doi:10.1126/science.aaw1720 (2019).

29 Zhang, Y. *et al.* Control of salicylic acid synthesis and systemic acquired resistance by two members of a plant-specific family of transcription factors. *Proc Natl Acad Sci U S A* **107**, 18220-18225 (2010).

30 Wang, L. *et al.* CBP60g and SARD1 play partially redundant critical roles in salicylic acid signaling. *Plant J* **67**, 1029-1041, doi:10.1111/j.1365-313X.2011.04655.x (2011).

31 Cheng, Y. T. *et al.* Stability of plant immune-receptor resistance proteins is controlled by SKP1-CULLIN1-F-box (SCF)-mediated protein degradation. *Proc Natl Acad Sci U S A* **108**, 14694-14699, doi:1105685108 [pii]10.1073/pnas.1105685108 (2011).

32 Liu, J. *et al.* The malectin-like receptor-like kinase LETUM1 modulates NLR protein SUMM2 activation via MEKK2 scaffolding. *Nature Plants* **6**, 1106-1115 (2020).

33 Dong, O. X. *et al.* Individual components of paired typical NLR immune receptors are regulated by distinct E3 ligases. *Nature plants* **4**, 699-710 (2018).

34 Zhang, Y. *et al.* TurboID-based proximity labeling reveals that UBR7 is a regulator of N NLR immune receptor-mediated immunity. *Nature communications* **10**, 1-17 (2019).

35 Wu, Z. *et al.* Plant E3 ligases SNIPER 1 and SNIPER 2 broadly regulate the homeostasis of sensor NLR immune receptors. *The EMBO journal* **39**, e104915 (2020).

36 Wan, W. L. *et al.* Comparing Arabidopsis receptor kinase and receptor protein‐mediated immune signaling reveals BIK1‐dependent differences. *New Phytologist* **221**, 2080-2095 (2019).

37 Li, F. *et al.* Modulation of RNA polymerase II phosphorylation downstream of pathogen perception orchestrates plant immunity. *Cell host & microbe* **16**, 748-758 (2014).

38 Kong, Q. *et al.* Two Redundant Receptor-Like Cytoplasmic Kinases Function Downstream of Pattern Recognition Receptors to Regulate Activation of SA Biosynthesis. *Plant Physiol* **171**, 1344-1354, doi:10.1104/pp.15.01954 (2016).

39 Rao, S. *et al.* Roles of receptor-like cytoplasmic kinase VII members in pattern-triggered immune signaling. *Plant physiology* **177**, 1679-1690 (2018).

40 Sreekanta, S. *et al.* The receptor-like cytoplasmic kinase PCRK1 contributes to pattern-triggered immunity against Pseudomonas syringae in Arabidopsis thaliana. *The New phytologist* **207**, 78-90, doi:10.1111/nph.13345 (2015).

41 Branon, T. C. *et al.* Efficient proximity labeling in living cells and organisms with TurboID. *Nature biotechnology* **36**, 880-887 (2018).

42 Ngou, B. P. M., Ahn, H.-K., Ding, P. & Jones, J. D. Mutual potentiation of plant immunity by cell-surface and intracellular receptors. *bioRxiv* (2020).

43 Yuan, M. *et al.* Pattern-recognition receptors are required for NLR-mediated plant immunity. *bioRxiv* (2020).

44 Tsuda, K., Sato, M., Stoddard, T., Glazebrook, J. & Katagiri, F. Network properties of robust immunity in plants. *PLoS Genet* **5**, e1000772 (2009).

45 Sun, T. *et al.* ChIP-seq reveals broad roles of SARD1 and CBP60g in regulating plant immunity. *Nature communications* **6**, 10159, doi:10.1038/ncomms10159 (2015).

46 Palma, K. *et al.* Autoimmunity in Arabidopsis acd11 Is Mediated by Epigenetic Regulation of an Immune Receptor. *PLoS pathogens* **6**, doi:ARTN e1001137 DOI 10.1371/journal.ppat.1001137 (2010).

47 Yi, H. & Richards, E. J. Phenotypic instability of Arabidopsis alleles affecting a disease Resistancegene cluster. *BMC plant biology* **8**, 36 (2008).

48 Kato, H., Saito, T., Ito, H., Komeda, Y. & Kato, A. Overexpression of the TIR-X gene results in a dwarf phenotype and activation of defense-related gene expression in Arabidopsis thaliana. *Journal of plant physiology* **171**, 382-388 (2014).

49 Swiderski, M. R., Birker, D. & Jones, J. D. The TIR domain of TIR-NB-LRR resistance proteins is a signaling domain involved in cell death induction. *Molecular plant-microbe interactions* **22**, 157-165 (2009).

50 Pruitt, R. N. *et al.* Arabidopsis cell surface LRR immune receptor signaling through the EDS1-PAD4-ADR1 node. *bioRxiv* (2020).

51 Wang, Z.-P. *et al.* Egg cell-specific promoter-controlled CRISPR/Cas9 efficiently generates homozygous mutants for multiple target genes in Arabidopsis in a single generation. *Genome biology* **16**, 144 (2015).

52 Liu, Y., Huang, X., Li, M., He, P. & Zhang, Y. Loss-of-function of Arabidopsis receptor-like kinase BIR1 activates cell death and defense responses mediated by BAK1 and SOBIR1. *The New phytologist* **212**, 637-645, doi:10.1111/nph.14072 (2016).

53 Xu, F. *et al.* Two N-terminal acetyltransferases antagonistically regulate the stability of a nod-like receptor in Arabidopsis. *Plant Cell* **27**, 1547-1562, doi:10.1105/tpc.15.00173 (2015).

54 Glazebrook, J., Rogers, E. E. & Ausubel, F. M. Isolation of Arabidopsis mutants with enhanced disease susceptibility by direct screening. *Genetics* **143**, 973-982 (1996).

55 Feys, B. J. *et al.* Arabidopsis SENESCENCE-ASSOCIATED GENE101 stabilizes and signals within an ENHANCED DISEASE SUSCEPTIBILITY1 complex in plant innate immunity. *Plant Cell* **17**, 2601-2613 (2005).

56 Li, X., Zhang, Y., Clarke, J. D., Li, Y. & Dong, X. Identification and cloning of a negative regulator of systemic acquired resistance, SNI1, through a screen for suppressors of npr1-1. *Cell* **98**, 329-339 (1999).

57 Bi, D., Cheng, Y. T., Li, X. & Zhang, Y. Activation of plant immune responses by a gain-of-function mutation in an atypical receptor-like kinase. *Plant Physiol* **153**, 1771-1779

(2010).

58 Li, L. *et al.* The FLS2-associated kinase BIK1 directly phosphorylates the NADPH oxidase RbohD to control plant immunity. *Cell Host Microbe* **15**, 329-338, doi:10.1016/j.chom.2014.02.009 (2014).

59 Zhang, R. *et al.* A high quality Arabidopsis transcriptome for accurate transcript-level analysis of alternative splicing. *Nucleic acids research* **45**, 5061-5073 (2017).

60 Patro, R., Duggal, G., Love, M. I., Irizarry, R. A. & Kingsford, C. Salmon provides fast and bias-aware quantification of transcript expression. *Nature methods* **14**, 417-419 (2017).

61 Soneson, C., Love, M. I. & Robinson, M. D. Differential analyses for RNA-seq: transcript-level estimates improve gene-level inferences. *F1000Research* **4** (2015).

62 Love, M. I., Huber, W. & Anders, S. Moderated estimation of fold change and dispersion for RNA-seq data with DESeq2. *Genome biology* **15**, 550 (2014).

63 Durinck, S., Spellman, P. T., Birney, E. & Huber, W. Mapping identifiers for the integration of genomic datasets with the R/Bioconductor package biomaRt. *Nature protocols* **4**, 1184 (2009).

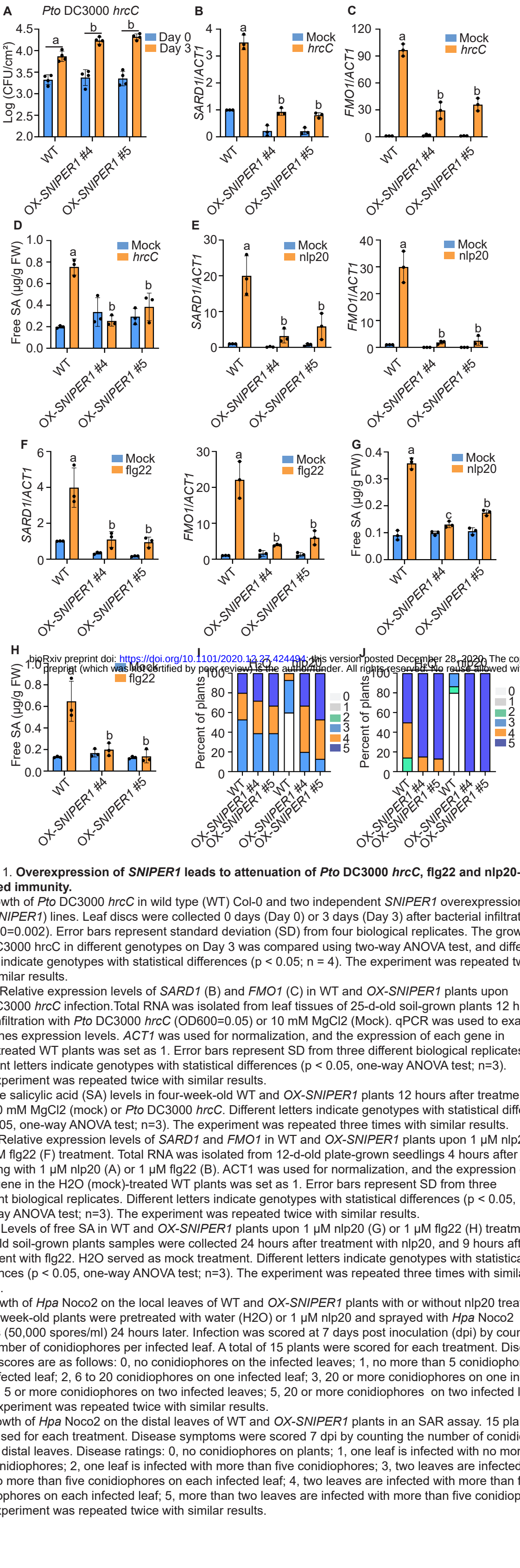

Figure 1. **Overexpression of *SNIPER1* leads to attenuation of *Pto* DC3000 *hrcC*, flg22 and nlp20-induced immunity.**

(A)Growth of *Pto* DC3000 *hrcC* in wild type (WT) Col-0 and two independent *SNIPER1* overexpression (*OX-SNIPER1*) lines. Leaf discs were collected 0 days (Day 0) or 3 days (Day 3) after bacterial infiltration (OD600=0.002). Error bars represent standard deviation (SD) from four biological replicates. The growth of Pto DC3000 hrcC in different genotypes on Day 3 was compared using two-way ANOVA test, and different letters indicate genotypes with statistical differences ($p < 0.05$; $n = 4$). The experiment was repeated twice with similar results.

(B, C) Relative expression levels of *SARD1* (B) and *FMO1* (C) in WT and *OX-SNIPER1* plants upon *Pto* DC3000 *hrcC* infection.Total RNA was isolated from leaf tissues of 25-d-old soil-grown plants 12 hours after infiltration with *Pto* DC3000 *hrcC* (OD600=0.05) or 10 mM MgCl2 (Mock). qPCR was used to examine the genes expression levels. *ACT1* was used for normalization, and the expression of each gene in mock-treated WT plants was set as 1. Error bars represent SD from three different biological replicates. Different letters indicate genotypes with statistical differences ($p < 0.05$, one-way ANOVA test; n=3). The experiment was repeated twice with similar results.

(D)Free salicylic acid (SA) levels in four-week-old WT and *OX-SNIPER1* plants 12 hours after treatment with 10 mM MgCl2 (mock) or *Pto* DC3000 *hrcC*. Different letters indicate genotypes with statistical differences ($p < 0.05$, one-way ANOVA test; n=3). The experiment was repeated three times with similar results.

(E, F) Relative expression levels of *SARD1* and *FMO1* in WT and *OX-SNIPER1* plants upon 1 µM nlp20 (E) or 1 µM flg22 (F) treatment. Total RNA was isolated from 12-d-old plate-grown seedlings 4 hours after spraying with 1 µM nlp20 (A) or 1 µM flg22 (B). ACT1 was used for normalization, and the expression of each gene in the H2O (mock)-treated WT plants was set as 1. Error bars represent SD from three different biological replicates. Different letters indicate genotypes with statistical differences ($p < 0.05$, one-way ANOVA test; n=3). The experiment was repeated twice with similar results.

(G, H) Levels of free SA in WT and *OX-SNIPER1* plants upon 1 µM nlp20 (G) or 1 µM flg22 (H) treatment. 25-d-old soil-grown plants samples were collected 24 hours after treatment with nlp20, and 9 hours after treatment with flg22. H2O served as mock treatment. Different letters indicate genotypes with statistical differences ($p < 0.05$, one-way ANOVA test; n=3). The experiment was repeated three times with similar results.

(I) Growth of *Hpa* Noco2 on the local leaves of WT and *OX-SNIPER1* plants with or without nlp20 treatment. Three-week-old plants were pretreated with water (H2O) or 1 µM nlp20 and sprayed with *Hpa* Noco2 spores (50,000 spores/ml) 24 hours later. Infection was scored at 7 days post inoculation (dpi) by counting the number of conidiophores per infected leaf. A total of 15 plants were scored for each treatment. Disease rating scores are as follows: 0, no conidiophores on the infected leaves; 1, no more than 5 conidiophores on one infected leaf; 2, 6 to 20 conidiophores on one infected leaf; 3, 20 or more conidiophores on one infected leaf; 4, 5 or more conidiophores on two infected leaves; 5, 20 or more conidiophores on two infected leaves. This experiment was repeated twice with similar results.

(J) Growth of *Hpa* Noco2 on the distal leaves of WT and *OX-SNIPER1* plants in an SAR assay. 15 plants were used for each treatment. Disease symptoms were scored 7 dpi by counting the number of conidiophores on the distal leaves. Disease ratings: 0, no conidiophores on plants; 1, one leaf is infected with no more than five conidiophores; 2, one leaf is infected with more than five conidiophores; 3, two leaves are infected but with no more than five conidiophores on each infected leaf; 4, two leaves are infected with more than five conidiophores on each infected leaf; 5, more than two leaves are infected with more than five conidiophores. The experiment was repeated twice with similar results.

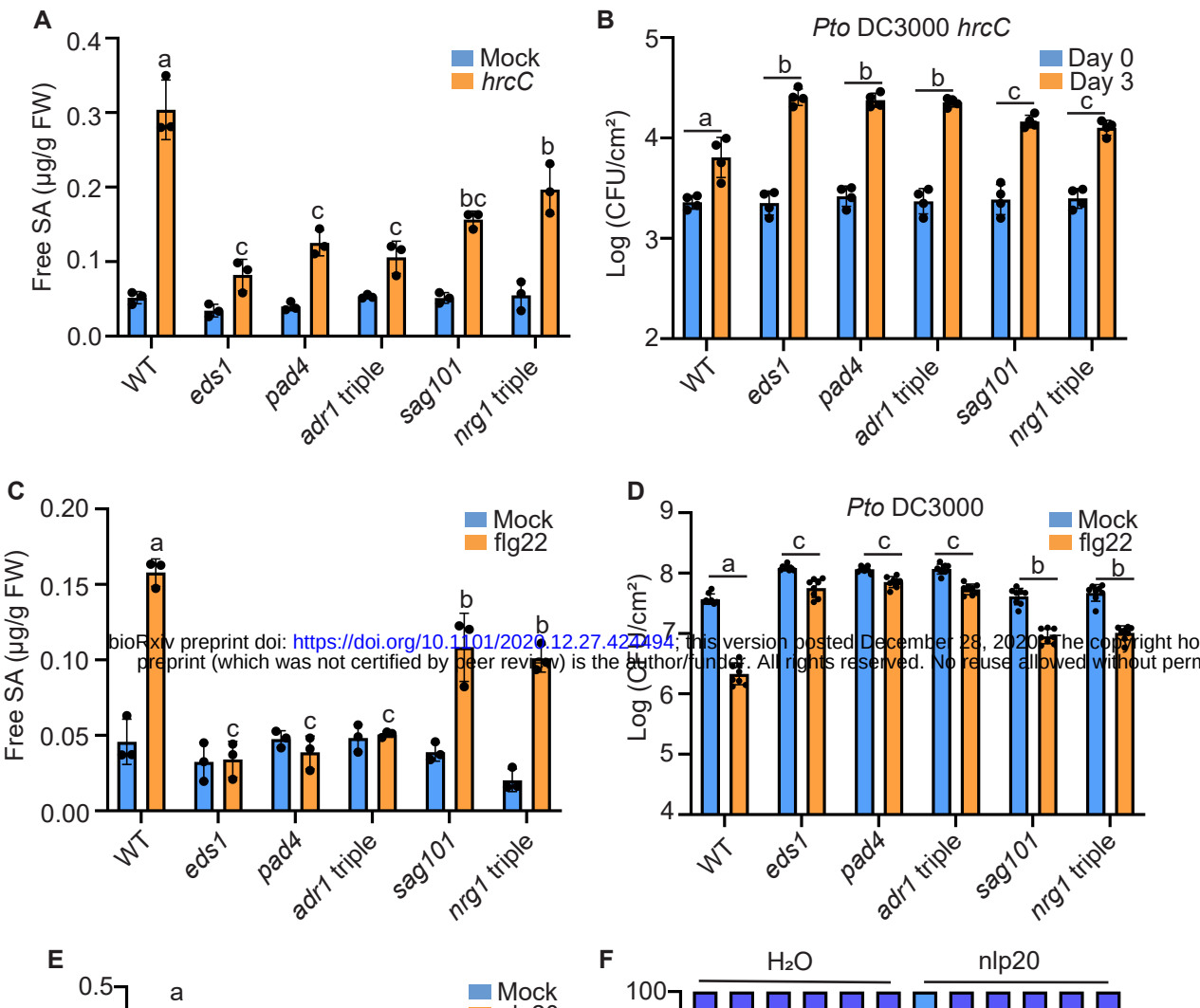

Figure 2. Contributions of TIR signaling components to *Pto* DC3000 *hrcC*, flg22 and nlp20-induced immunity.

(A) Levels of free SA in four-week-old soil-grown WT, *eds1-24*, *pad4-1*, *sag101-1*, *adr1* triple and *nrg1* triple mutants 12 hours after treatment with 10 mM MgCl2 or *Pto* DC3000 *hrcC* (OD600=0.05) for 12 hours. Different letters indicate genotypes with statistical differences ($p < 0.05$, one-way ANOVA test; n=3). The experiment was repeated three times with similar results.

(B) Growth of *Pto* DC3000 *hrcC* in 25-day-old soil-grown plants of the indicated genotypes. Leaf discs were collected 0 days (Day 0) or 3 days (Day 3) after Pto DC3000 hrcC (OD600=0.002) infiltration. Error bars represent SD from four biological replicates. The growth of *Pto* DC3000 *hrcC* in different genotypes was compared using two-way ANOVA test, and different letters indicate genotypes with statistical differences ($p < 0.05$, $n = 4$). The experiment was repeated twice with similar results.

(C) Levels of free SA in four-week-old soil-grown plants of the indicated genotypes after treatment with water or 1 µM flg22 for 9 hours. Different letters indicate genotypes with statistical differences ($p < 0.05$, one-way ANOVA test; n=3). The experiment was repeated three times with similar results.

(D) Growth of *Pto* DC3000 in the leaves of four-week-old WT, *eds1-24*, *pad4-1*, *sag101-1*, *adr1* triple and *nrg1* triple mutant plants after treatment with water or 1 µM flg22. 24 hours later, the same treated leaves were infiltrated with *Pto* DC3000. Samples were taken 3 days after *Pto* DC3000 inoculation. Error bars represent SD from six biological replicates. The flg22-induced protection among different genotypes was compared using two-way ANOVA test, and different letters indicate genotypes with statistical differences ($p < 0.05$, $n= 6$). The experiment was repeated twice with similar results.

(E) Levels of free SA in four-week-old soil-grown plants of the indicated genotypes after treatment with water (mock) or 1 µM nlp20 for 24h. Different letters indicate genotypes with statistical differences ($p < 0.05$, one-way ANOVA test; n=3). The experiment was repeated three times with similar results.

(F) Growth of *Hpa* Noco2 on the local leaves of the indicated plants. Three-week-old soil-grown plants were pretreated with water or 1 µM nlp20 and sprayed with Hpa Noco2 spores (50,000 spores/ml) 24 hours later. Disease ratings are as described in Fig 1. The experiment was repeated twice with similar results.

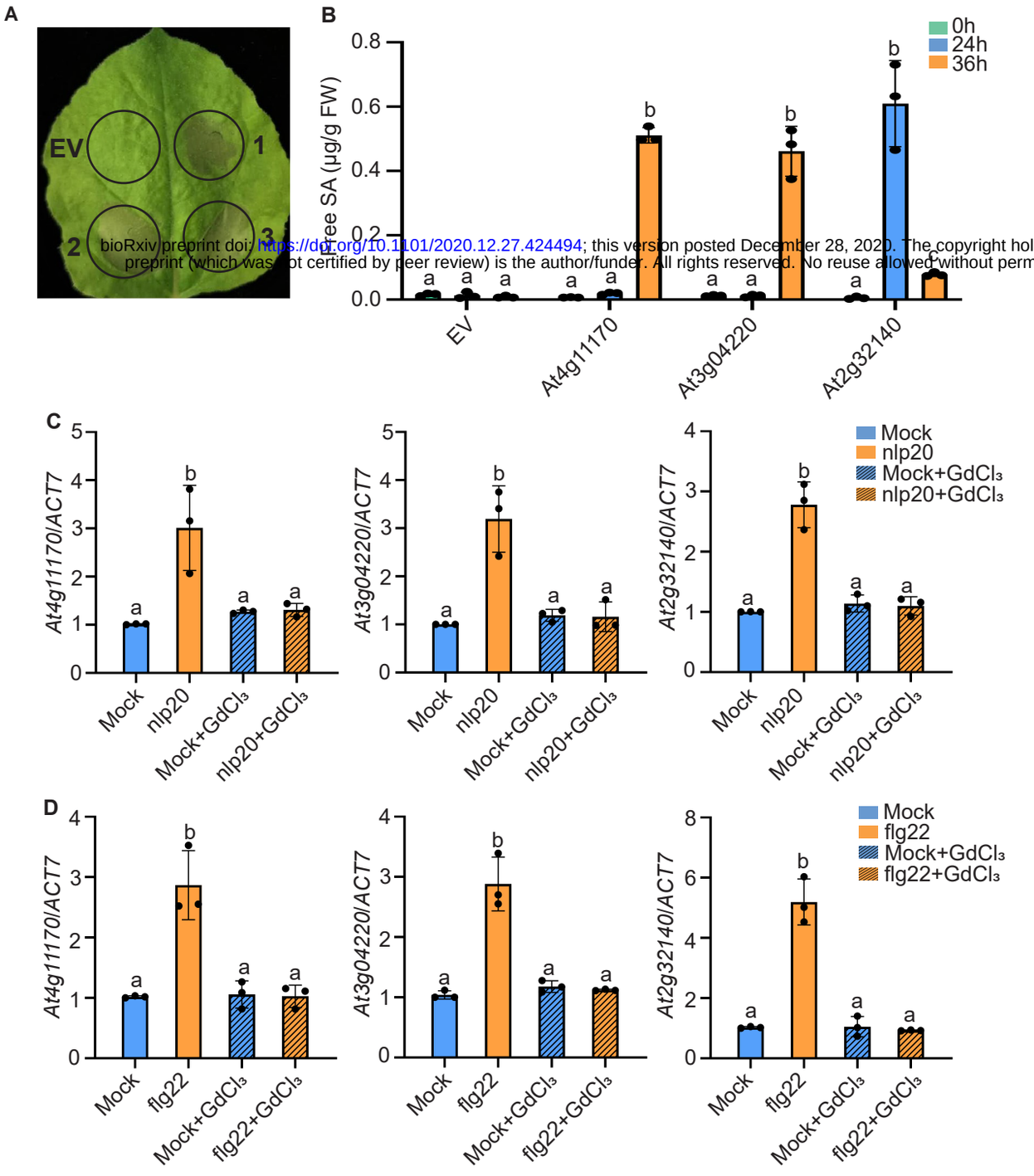

Figure 3. Overexpression of *TIR* genes activates SA biosynthesis in *N. benthamiana*.
(A) Hypersensitive response (HR) in the *N. benthamiana* leaves expressing the *TIR* genes *At4g11170*, *At3g04220* or *At2g32140* through *Agrobacterium tumefaciens* GV3101 (OD600=0.4) infiltration. Photographs were taken 3 days after Agrobacterium infiltration. The empty vector (EV) treatment serves as control; 1, *At4g11170*; 2, *At3g04220*; 3, *At2g32140*.
(B) Levels of free SA in *N. benthamiana* leaves after infiltration of *Agrobacterium* (OD600=0.4) carrying the *TIR* genes from (A). Samples were collected 24 and 36 hours post infiltration, before HR was visible. Error bars represent SD from three biological replicates. Different letters indicate different time course with statistical differences ($p < 0.05$, one-way ANOVA test; n=3).
(C, D) Induction of the indicated *TIR* genes by nlp20 (C) or flg22 (D). Ten-day-old plate-grown WT plants were transplanted to water 1 day before for recovery and then pretreated with water (Mock) or 100 μM GdCl3 for 1 hour. Samples were collected 1 hour after supplying with 1 μM nlp20 or 1 μM flg22. qPCR was used to examine the genes expression level. *ACT7* was used for normalization. Error bars represent SD from three different biological replicates. Different letters indicate different treatment with statistical differences ($p < 0.05$, one-way ANOVA test; n=3) All the experiments were repeated twice with similar results.

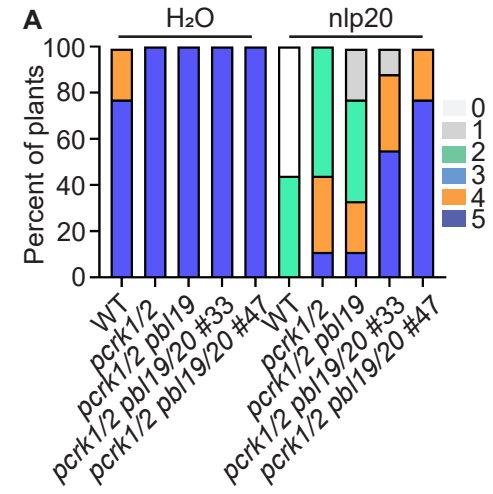

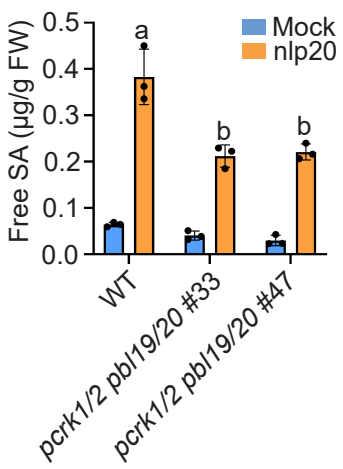

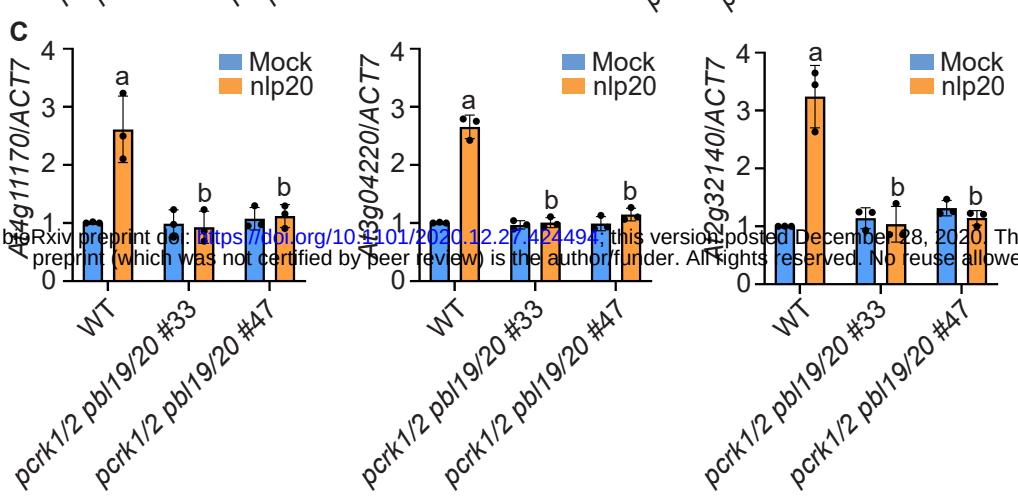

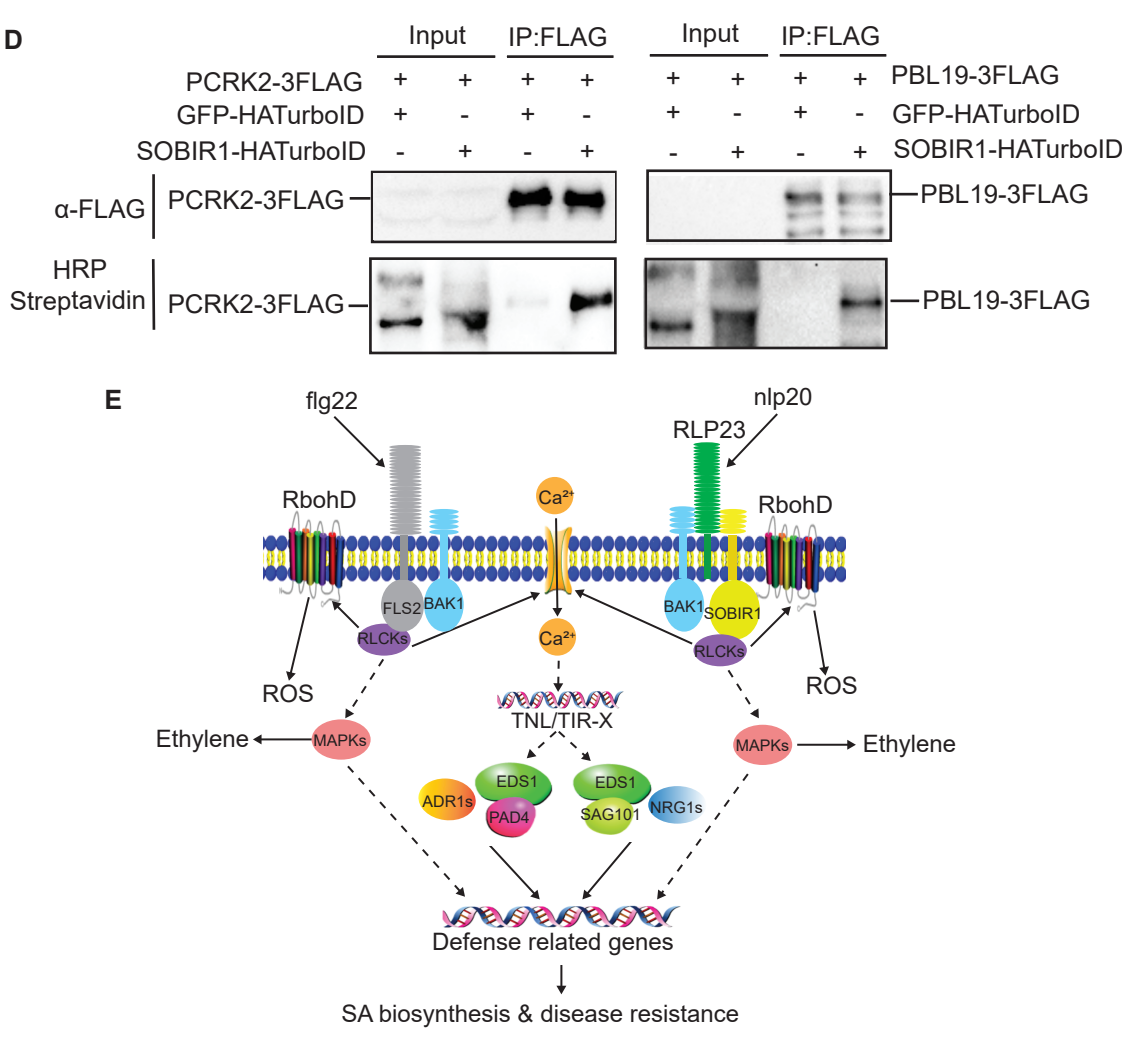

Figure 4. PCRK1/2 and PBL19/20 are required for nlp20-induced immunity.
(A) Growth of *Hpa* Noco2 on the distal leaves of WT, *pcrk1/2*, *pcrk1/2 pbl19*, *pcrk1/2 pbl19/20* #33 and *pcrk1/2 pbl19/20* #47 quadruple mutant plants. 21-d-old soil-grown plants were treated with 1 μM nlp20 and sprayed *Hpa* Noco2 spores (50,000 spores/ml) 24 hours later. The detail method was described in Fig 2F.
(B) Levels of free SA in four-week-old soil-grown plants of the indicated genotypes treated with water or 1 μM nlp20. Samples were collected 24 hours post elicitor treatment. Different letters indicate genotypes with statistical differences ($p < 0.05$, one-way ANOVA test; n=3).
(C) The induction of *At4g11170*, *At3g04220* and *At2g32140* (*TIR* genes) in the indicated genotypes. Total RNA was isolated from seedlings of 10-d-old plate-grown plants 1 h after treatment with 1 μM nlp20. *ACT7* was used for normalization, and the expression of each gene in mock-treated WT was set as 1. Error bars represent SD from three different biological replicates. Different letters indicate genotypes with statistical differences ($p < 0.05$, one-way ANOVA test; n=3).
(D) Immunoprecipitation and biotinylation of PCRK2/PBL19-3FLAG by SOBIR1-HATurboID in *N. benthamiana*. *Agrobacterium* carrying the indicated constructs were infiltrated into *N. benthamiana* leaves for protein expression. Immunoprecipitation was carried out with anti-FLAG beads. The 3FLAG-tagged proteins were detected using an anti-FLAG antibody. The biotinylated proteins were detected using HRP-Streptavidin. The experiments in (A-D) were repeated twice with similar results.
(E) A working model for the contribution of TIR signaling in PTI. Upon perception of pathogen elicitors such as flg22 and nlp20, PRRs activate early immune responses such as ROS production, MAPK activation and Ca2+ influx through RLCKs. Elevated cytosolic Ca2+ levels induce the expression of a large number of TIR genes, leading to activation of downstream defense pathways through the EDS1/PAD4/ADR1s and EDS1/SAG101/NRG1s signaling modules. Activation of TIR signaling further induces downstream defense gene expression, resulting in increased SA biosynthesis and enhanced resistance to pathogens. In parallel, activation of MAPKs promotes the biosynthesis of ethylene.

figure S1

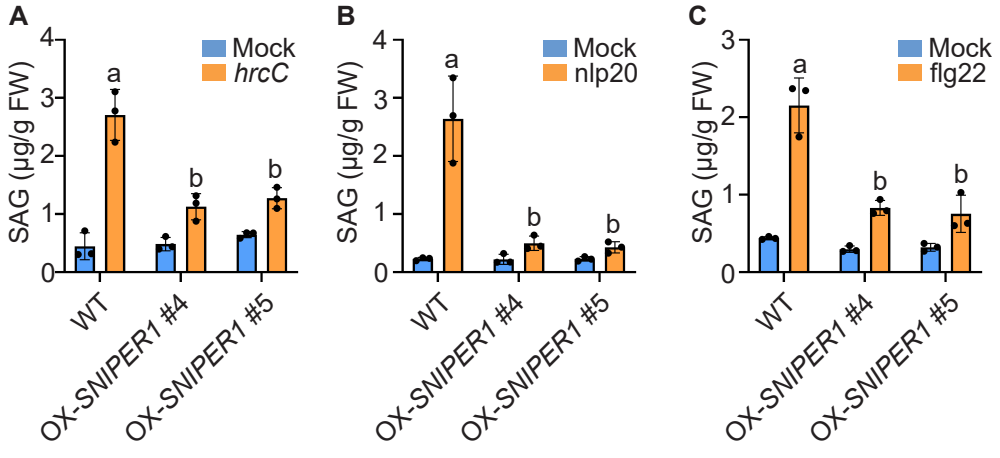

Figure S1. Levels of glucose-conjugated SA (SAG) in WT and OX-SNIPER1 plants.
(A) SAG levels in four-week-old soil-grown WT and OX-SNIPER1 plants treated with 10 mM MgCl2 (mock) or Pto DC3000 hrcC.
(B, C) SAG levels in 25-d-old plants WT and OX-SNIPER1 plants treated with H2O (mock), 1 µM nlp20 (B) or 1 µM flg22 (C). Samples were collected for SAG measurement 24 hr after 1µM nlp20, or 9 hr after 1µM flg22 treatment. Different letters indicate genotypes with statistical differences ($p < 0.05$, one-way ANOVA test; n=3).
All the experiments were repeated three times with similar results.

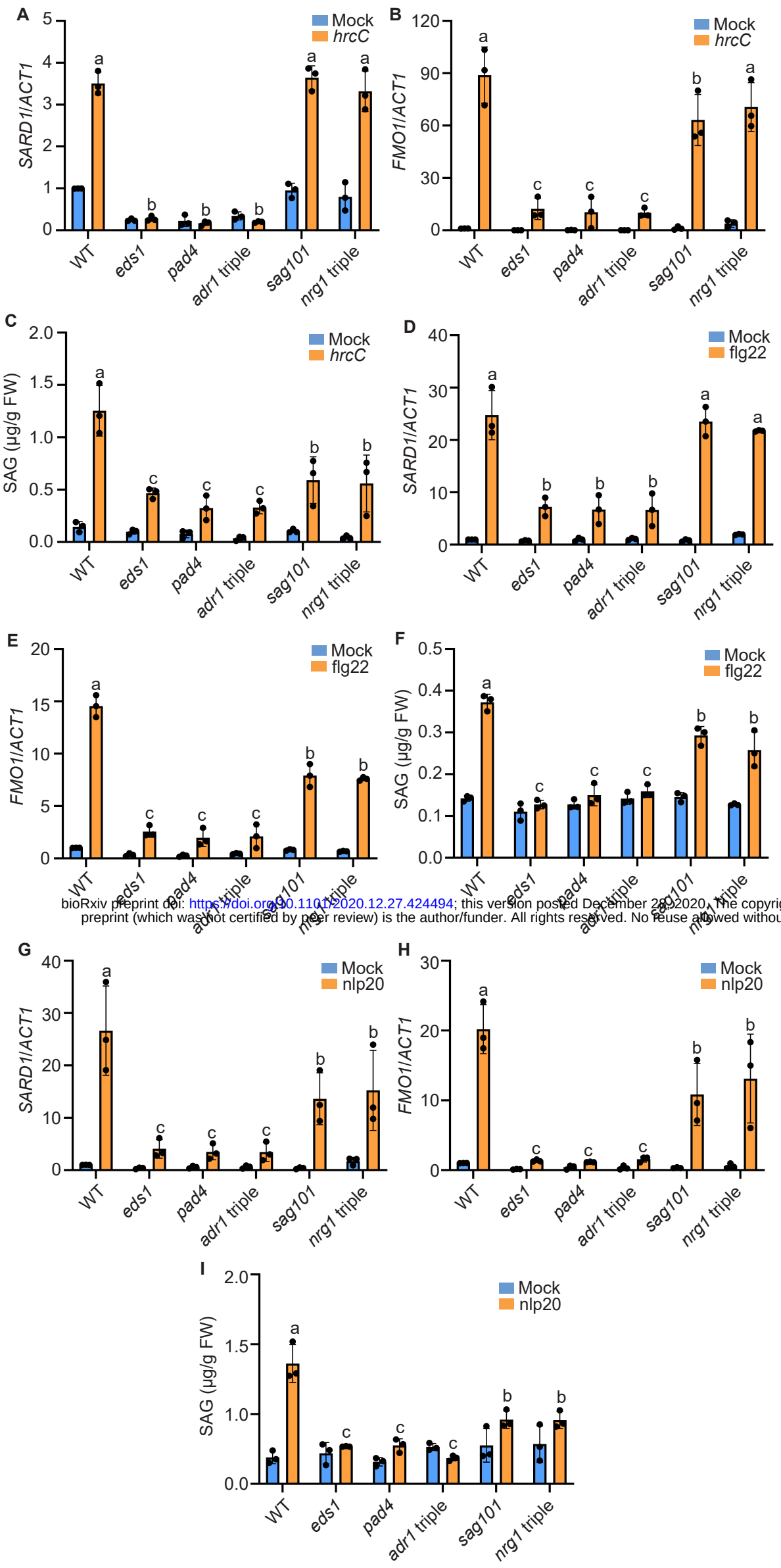

Figure S2. Induction of *SARD1* and *FMO1* gene expression and SAG production in TIR signaling mutants upon *Pto* DC3000 *hrcC*, flg22 or nlp20 treatment.

(A, B) Relative expression levels of *SARD1* (A) and *FMO1* (B) in WT, *eds1-24*, *pad4-1*, *sag101-1*, *adr1 adr-L1 adr-L2* (*adr1* triple) and *nrg1a nrg1b nrg1c* (*nrg1* triple) mutant plants after treatment with *Pto* DC3000 *hrcC* (OD600 = 0.05) for 12 hours. Error bars represent SD from three different biological replicates. Different letters indicate genotypes with statistical differences ($p < 0.05$, one-way ANOVA test; n=3).

(C, F, I) Four-week-old soil-grown plants of the indicated genotypes were treated with *Pto* DC3000 *hrcC* (OD600=0.05) (D), 1 µM flg22 (F) or 1 µM nlp20 (I). Samples were collected for SAG measurement 12 hr after inoculation of *Pto* DC3000 *hrcC*, 24 hr after treatment with 1 µM nlp20, or 9 hr after treatment with 1 µM flg22. Different letters indicate genotypes with statistical differences ($p < 0.05$, one-way ANOVA test; n=3). The experiment was repeated three times with similar results.

(D, E) Relative expression levels of *SARD1* (D) and *FMO1 (*E) in the indicated genotypes upon flg22 treatment. Total RNA was isolated from 12-d-old plate-grown seedlings 4 h after spraying with 1 µM flg22. Different letters indicate genotypes with statistical differences ($p < 0.05$, one-way ANOVA test; n=3).

(G, H) Relative expression levels of *SARD1* (G) and *FMO1* (H) in the indicated genotypes upon nlp20 treatment. Total RNA was isolated from 12-d-old plate-grown seedlings 4 h after spraying with 1 µM nlp20. Different letters indicate genotypes with statistical differences ($p < 0.05$, one-way ANOVA test; n=3).

For gene expression analysis in (A, B, D, E, G, H), the expression of each gene in the mock-treated WT plants was set as 1. All gene expression analyses were repeated twice with similar results.

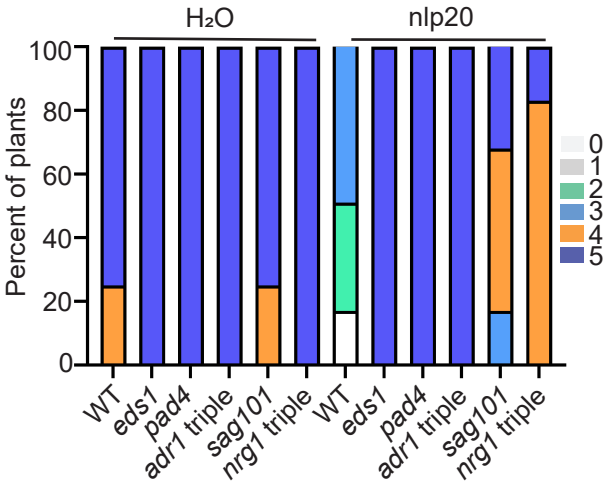

Figure S3. Growth of *Hpa* Noco2 on the distal leaves of TIR signaling mutants. mutants.
Three-week-old soil-grown plants were pretreated with water or 1 μM nlp20 and sprayed with *Hpa* Noco2 spores (50,000 spores/ml) 24 hours later. Disease ratings are as described in Fig 1. The experiment was repeated twice with similar results.

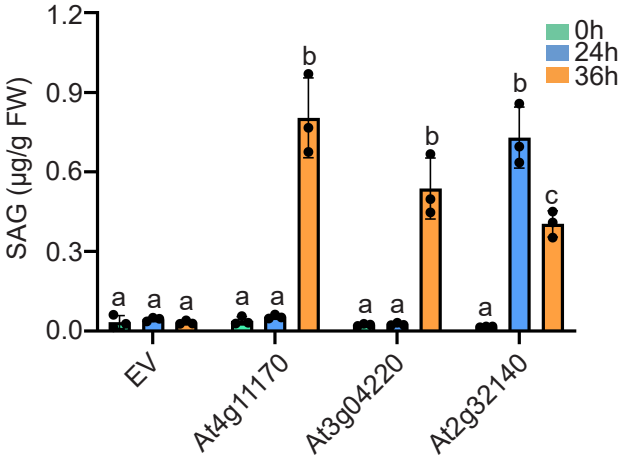

Figure S4. Levels of glucose-conjugated SA (SAG) in *N. benthamiana* leaves after infiltration of *Agrobacterium* carrying the *TIR* genes.
Samples were collected 24 and 36 hours post infiltration of the bacteria (OD600=0.4) before HR was visible. Different letters indicate statistical differences ($p < 0.05$, one-way ANOVA test; n=3) compared with the empty vector control. The experiment was repeated twice with similar results.

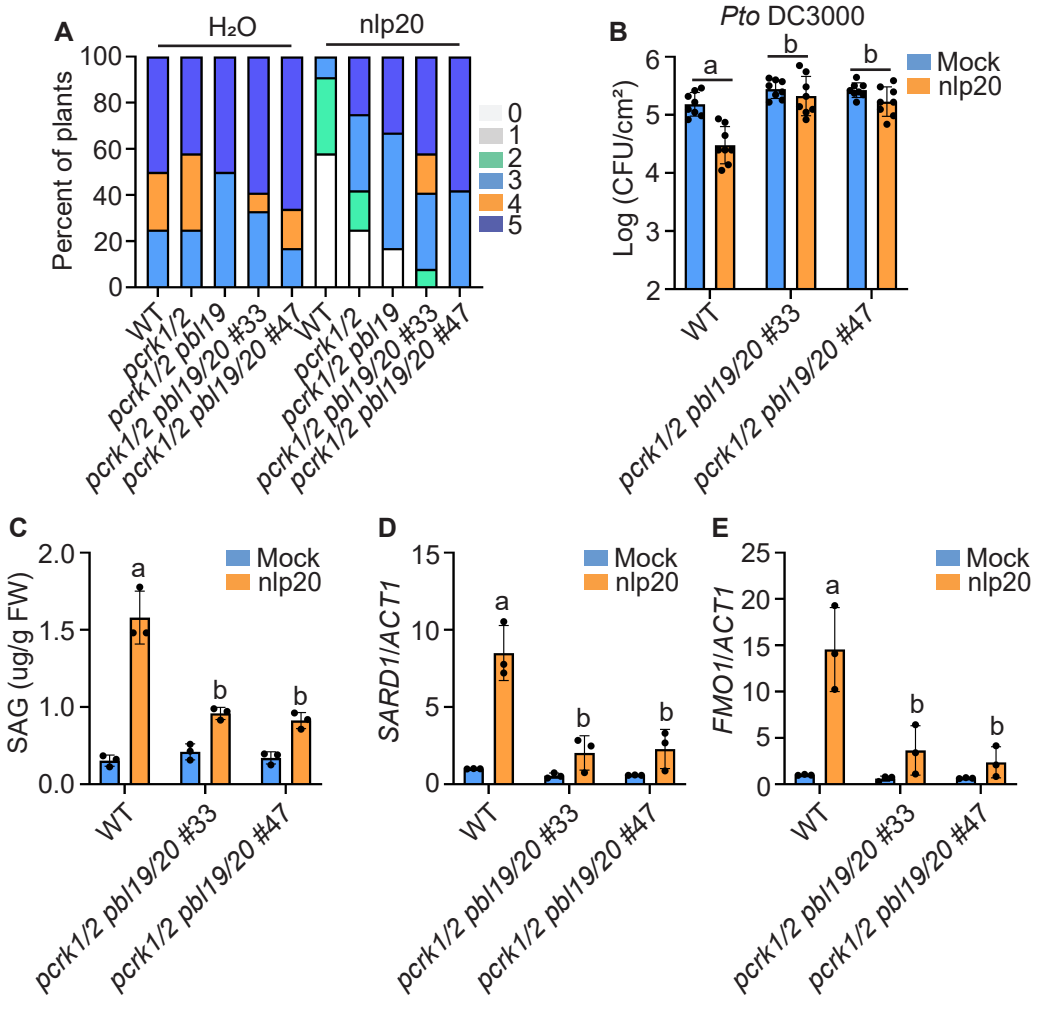

Figure S5. nlp20-induced immune responses are compromised in *pcrk1/2 pbl19/20* quadruple mutant plants.

(A) Growth of *Hpa* Noco2 on the local leaves of WT, *pcrk1/2*, *pcrk1/2 pbl19*, *pcrk1/2 pbl19/20* #33 and *pcrk1/2 pbl19/20* #47 quadruple mutant plants after 1 μM nlp20 treatment. Infection was scored 7 dpi by counting the number of conidiophores per infected leaf. Detailed methodology was described in Fig 2E.

(B) Growth of *Pto* DC3000 in the leaves of four-week-old WT, *pcrk1/2 pbl19/20* #33 and *pcrk1/2 pbl19/20* #47 quadruple mutant plants pre-treated with water or 1 μM nlp20. 24 hours post elicitor treatment, the treated leaves were infiltrated with Pto DC3000 (OD600=0.001). Samples were taken 3 days after *Pto* DC3000 inoculation. Error bars represent SD from six biological replicates. The nlp20-induced protection among different genotypes was compared using two-way ANOVA test, and different letters indicate genotypes with statistical differences ($p < 0.05$, n= 6).

(C) Levels of SAG in four-week-old soil-grown plants of the indicated genotypes treated with water or 1 μM nlp20. Samples were collected 24 hours post elicitor treatment. Different letters indicate statistical differences ($p < 0.05$, one-way ANOVA test; n=3).

(D, E) Relative expression levels of *SARD1* (D) and *FMO1* (E) in the indicated genotypes. Total RNA extracted from 12-d-old plate-grown plants treated with 1 μM nlp20 for 4h. *ACT1* was used for normalization, and the expression of each gene in mock-treated WT was set as 1. Error bars represent SD from three different biological replicates. Different letters indicate genotypes with statistical differences ($p < 0.05$, one-way ANOVA test; n=3).

All the experiments were repeated twice with similar results.

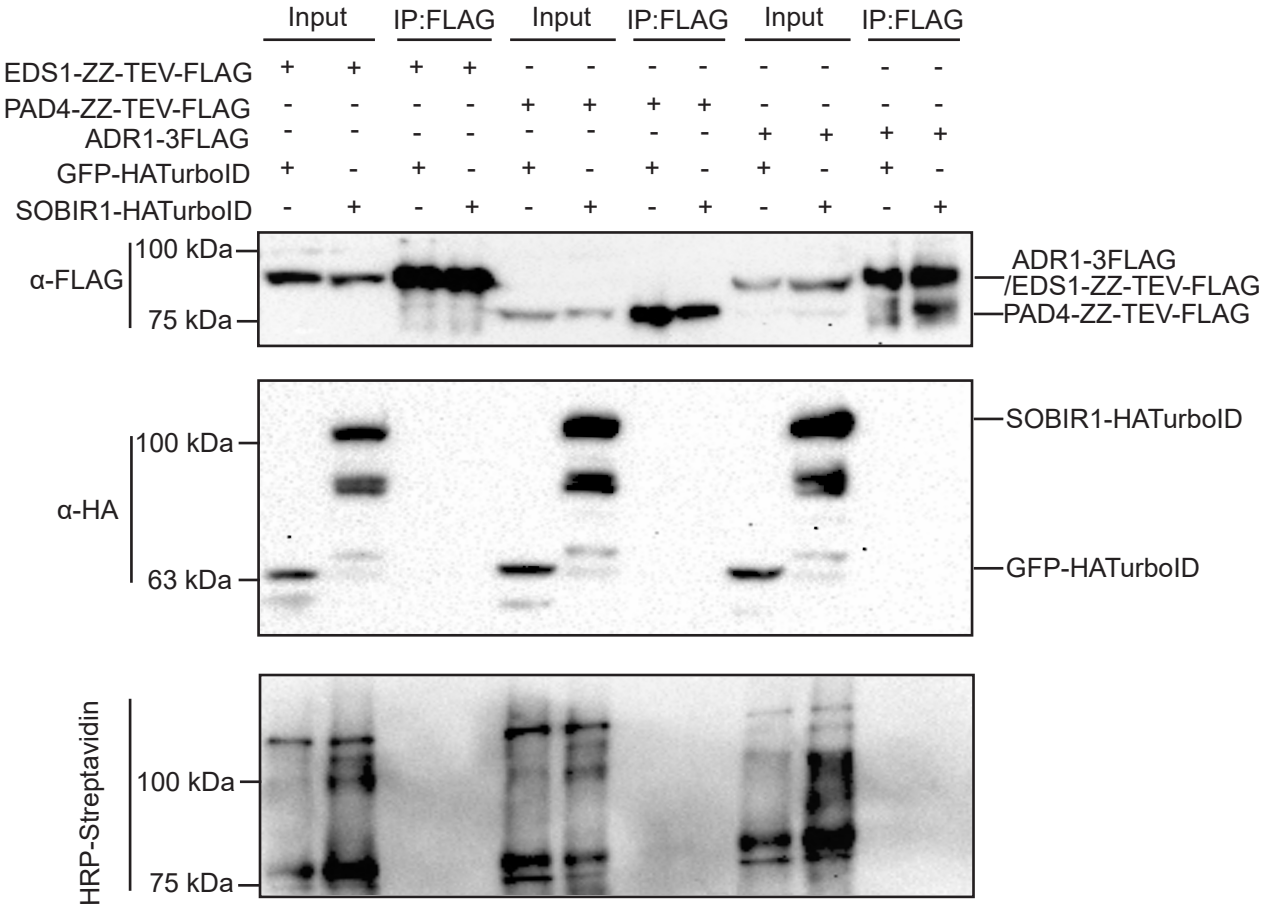

Figure S6. Analysis of interactions between SOBIR1 and EDS1/PAD4/ADR1 by TurboID and co-immunoprecipitation analysis.

Agrobacterium carrying the indicated constructs were infiltrated into N. benthamiana leaves for protein expression. Immunoprecipitation of EDS1-FLAG-ZZ, PAD4-FLAG-ZZ or ADR1-3FLAG was carried out with anti-FLAG beads. The 3FLAG-tagged and HATurboID fusion proteins were detected by western blot using an anti-FLAG or anti-HA antibody by western blot. The biotinylated proteins were detected by western blot using HRP-Streptavidin. Molecular mass marker in kiloDaltons is indicated on the left. The experiment was repeated twice with similar results.

Table S1. TIR-domain containing genes induced by nlp20 treatment for 1 hour compared with H_2O treatment for 1 hour.

Gene ID	Log2(Fold Change)	Adjusted p-value	Gene Name	Description
AT1G66090	4.182314	2.11E-10		Disease resistance protein (TIR-NBS class)
AT2G32140	3.410955	6.12E-04		Transmembrane receptor
AT3G04220	2.978868	5.65E-06		Disease resistance protein (TIR-NBS-LRR class) family
AT5G41750	2.702796	1.29E-04		Disease resistance protein (TIR-NBS-LRR class) family
AT3G04210	2.613868	1.24E-08		At3g04210/T6K12_17
AT2G20142	2.309786	1.93E-03		Toll-Interleukin-Resistance (TIR) domain family protein
AT4G19520	2.105768	7.57E-06		Probable disease resistance protein At4g19520
AT5G22690	1.954292	1.70E-05		Disease resistance protein (TIR-NBS-LRR class) family
AT1G72900	1.927421	1.63E-03		Similar to part of disease resistance protein
AT1G17600	1.866072	1.21E-04		Disease resistance protein (TIR-NBS-LRR class) family
AT1G65390	1.706482	1.64E-03	PP2A5	Protein PHLOEM PROTEIN 2-LIKE A5
AT2G16870	1.65859	4.47E-04		Disease resistance protein (TIR-NBS-LRR class) family
AT5G44870	1.635193	7.33E-07	LAZ5	Disease resistance protein LAZ5
AT1G56540	1.63069	2.20E-04		Disease resistance protein (TIR-NBS-LRR class) family
AT5G41740	1.585872	1.39E-03		Disease resistance protein (TIR-NBS-LRR class) family
AT4G36150	1.514324	2.73E-03		Disease resistance protein (TIR-NBS-LRR class) family
AT4G16960	1.493714	5.81E-04		Disease resistance protein (TIR-NBS-LRR class) family
AT1G72940	1.456181	4.55E-03		At1g72940/F3N23_14
AT5G46510	1.382137	1.87E-04		Disease resistance protein (TIR-NBS-LRR class) family
AT5G46470	1.323092	5.59E-05	RPS6	Disease resistance protein RPS6
AT4G16860	1.316684	2.28E-03	RPP4	Disease resistance protein RPP4
AT3G44630	1.296601	3.67E-03		Disease resistance protein (TIR-NBS-LRR class) family
AT4G36140	1.190924	1.25E-04		Disease resistance protein (TIR-NBS-LRR class)
AT1G31540	1.073651	9.72E-04		Disease resistance protein (TIR-NBS-LRR class) family
AT5G45250	1.06893	1.61E-03	RPS4	Disease resistance protein RPS4
AT4G16890	0.86282	4.61E-03	SNC1	disease resistance protein (TIR-NBS-LRR class), putative

Table S2. TIR-domain containing genes induced by nlp20 treatment for 6 hours compared with H_2O treatment for 6 hours.

Gene ID	Log2(Fold Change)	Adjusted p-value	Gene Name	Description
AT1G57630	7.14555	3.84E-06		Disease resistance protein RPP1-WsB, putative
AT4G11170	4.73465	4.44E-04		Putative disease resistance protein At4g11170
AT5G45090	3.91362	1.51E-02	PP2A7	Uncharacterized protein PHLOEM PROTEIN 2-LIKE A7
AT1G47370	3.62641	2.83E-02		Toll-Interleukin-Resistance (TIR) domain family protein
AT2G32140	3.59523	1.72E-02		Transmembrane receptor
AT5G41750	3.33276	2.23E-04		Disease resistance protein (TIR-NBS-LRR class) family
AT1G66090	3.02848	4.22E-04		Disease resistance protein (TIR-NBS class)
AT1G72920	2.84247	3.10E-03		Similar to part of disease resistance protein
AT5G45000	2.74362	1.49E-02		Disease resistance protein (TIR-NBS-LRR class) family
AT2G20142	2.4793	2.51E-02		Toll-Interleukin-Resistance (TIR) domain family protein
AT3G04220	2.28377	2.68E-02		Disease resistance protein (TIR-NBS-LRR class) family
AT5G58120	1.90423	9.43E-03		Disease resistance protein (TIR-NBS-LRR class) family
AT5G41740	1.71984	1.75E-02		Disease resistance protein (TIR-NBS-LRR class) family
AT1G72900	1.71688	8.78E-02		Similar to part of disease resistance protein

Table S3. TIR-domain containing genes induced by flg22 treatment for 30 min compared with untreated*.

Gene ID	Log2(Fold Change)	Adjusted p-value	Gene Name	Description
AT1G66090	23.2	2.52E-54		Disease resistance protein (TIR-NBS class)
AT1G65390	19.4	0.00E+00	PP2A5	Protein PHLOEM PROTEIN 2-LIKE A5
AT4G19520	12.3	0.00E+00		Probable disease resistance protein At4g19520
AT5G41750	12.3	2.09E-168		Disease resistance protein (TIR-NBS-LRR class) family
AT5G41740	11.6	3.96E-217		Disease resistance protein (TIR-NBS-LRR class) family
AT1G72900	10	3.40E-31		Similar to part of disease resistance protein
AT2G32140	8.9	1.59E-31		Transmembrane receptor
AT2G20142	8.8	1.73E-08		Toll-Interleukin-Resistance (TIR) domain family protein
AT4G14370	8.4	1.20E-76		Disease resistance protein (TIR-NBS-LRR class) family
AT5G44910	6	5.36E-23		Similarity to disease resistance protein
AT4G11170	5.7	5.69E-09		Putative disease resistance protein At4g11170
AT1G51270	5.7	3.59E-66		Vesicle-associated protein 1-4
AT1G63860	5.5	8.73E-63		Disease resistance protein (TIR-NBS-LRR class) family
AT5G22690	5.3	9.39E-61		Disease resistance protein (TIR-NBS-LRR class) family
AT1G63750	5.1	5.65E-42		Disease resistance protein (TIR-NBS-LRR class) family
AT3G04220	4.8	1.52E-08		Disease resistance protein (TIR-NBS-LRR class) family
AT1G72920	4.3	1.41E-15		Similar to part of disease resistance protein
AT1G57630	4.3	1.46E-04		Disease resistance protein RPP1-WsB, putative
AT1G56540	3.9	1.62E-11		Disease resistance protein (TIR-NBS-LRR class) family
AT3G44630	3.9	9.70E-104		Disease resistance protein (TIR-NBS-LRR class) family
AT1G56510	3.9	8.21E-75	ADR2	Disease resistance protein ADR2
AT1G72940	3.7	1.46E-36		At1g72940/F3N23_14
AT4G16960	3.6	1.53E-31		Disease resistance protein (TIR-NBS-LRR class) family
AT3G04210	3.4	2.85E-11		At3g04210/T6K12_17

AT1G31540	3.3	2.24E-46		Disease resistance protein (TIR-NBS-LRR class) family
AT5G58120	3.3	8.42E-38		Disease resistance protein (TIR-NBS-LRR class) family
AT5G46470	3.2	4.95E-73	RPS6	Disease resistance protein RPS6
AT1G72910	3.1	1.35E-29		Similar to part of disease resistance protein
AT4G16860	3	7.19E-62	RPP4	Disease resistance protein RPP4
AT1G72930	2.7	5.91E-48	TIR	Toll/interleukin-1 receptor-like protein
AT5G46510	2.7	1.22E-33		Disease resistance protein (TIR-NBS-LRR class) family
AT4G16940	2.5	1.31E-07		Disease resistance protein (TIR-NBS-LRR class) family
AT5G46520	2.4	5.56E-17		Disease resistance protein (TIR-NBS-LRR class) family
AT5G40910	2.4	1.88E-31		Disease resistance protein (TIR-NBS-LRR class) family
AT3G44400	2.3	3.00E-04		Disease resistance protein (TIR-NBS-LRR class) family
AT1G56520	2.2	3.45E-08		Disease resistance protein (TIR-NBS-LRR class) family
AT1G17600	2.1	2.21E-02		Disease resistance protein (TIR-NBS-LRR class) family
AT5G45070	2	3.02E-02	PP2A8	Protein PHLOEM PROTEIN 2-LIKE A8
AT5G11250	2	8.32E-06		Disease resistance protein (TIR-NBS-LRR class)
AT2G16870	1.9	9.09E-02		Disease resistance protein (TIR-NBS-LRR class) family
AT5G41550	1.9	2.70E-01		Disease resistance protein (TIR-NBS-LRR class) family
AT5G44870	1.9	1.07E-10	LAZ5	Disease resistance protein LAZ5
AT4G16890	1.8	2.93E-22	SNC1	Disease resistance protein (TIR-NBS-LRR class), putative
AT3G44480	1.7	5.62E-17	RPP1	Disease resistance protein (TIR-NBS-LRR class) family
AT1G72950	1.7	6.74E-01		Disease resistance protein (TIR-NBS class)
AT1G63740	1.7	3.23E-02		Disease resistance protein (TIR-NBS-LRR class) family

*subset directly from Li et al., 2015 Cell Host and Microbe. DOI:10.1016/j.chom.2014.10.018

Table S4. Sequences of primers used in this study.

Primer	5’-3’ sequence	purpose
PCRK1-F	GAAGTGAATGCAGAACTTAC	genotyping
PCRK1-R	GAGAATCGCCCAAGATGCAG	genotyping
PCRK2-F	TTGGTGATCTTAAATCTGCC	genotyping
PCRK2-R	ACCAAGTTTGAATGCTCGAC	genotyping
PBL19-F	TCCATCAAAATTCCACTGGTT	genotyping
PBL19-R	AACCAAAAGCCTCTCGATCC	genotyping
EDS1-DelPCR-F	AGAACGTAAGACAGGGTTTG	genotyping
EDS1-DelPCR-R	GATGGAGTCTATATTAAAGAGACG	genotyping
EDS1-Pres-F	ACAAGCCAAAGTGTCAAGCC	genotyping
EDS1-Pres-R	CAAGCATCCCTTCTAATGTC	genotyping
Actin1-F	CGATGAAGCTCAATCCAAACGA	RT-PCR
Actin1-R	CAGAGTCGAGCACAATACCG	RT-PCR
SARD1-RT-F	TCAAGGCGTTGTGGTTTGTG	RT-PCR
SARD1-RT-R	CGTCAACGACGGATAGTTTC	RT-PCR
FMO1-RT-F	TGCCTTTATACAGGGGAACA	RT-PCR
FMO1-RT-R	TGGAAATGCAATGACGTTTG	RT-PCR
EDS1-BsF	ATATATGGTCTCGATTGCTAACCGAGCGCTATCACAGTT	pHEE401E
EDS1-F0	TGCTAACCGAGCGCTATCACAGTTTTAGAGCTAGAAATAGC	pHEE401E
EDS1-R0	AACAAGGGAGATGTATTCTCCGCAATCTCTTAGTCGACTCTAC	pHEE401E
EDS1-BsR	ATTATTGGTCTCGAAACAAGGGAGATGTATTCTCCGC	pHEE401E
PBL20-DT1-BsF0	ATATATGGTCTCGATTGCCAAAATCCAGAGGAAATAGTTTTAGAGCTAGAAATAG	pHEE401E
PBL20-DT2-BsR0	ATTATTGGTCTCGAAACTAGCAATTGGATACTTATTCAATCTCTTAGTCGACTCTA	pHEE401E
PCRK2-Kpn1-F	CCGGGGTACCATGAAATGCTTCTTATTCCCTCT	pBASTA-35S-3FLAG

PCRK2-spe1-R	AAAGAATGTGAGAGCTTGTACTAGTAGGCCTAGA	pBASTA-35S-3FLAG
PBL19-Kpn1-F	CCGGGGTACCATGAACTGTCTGTTCTTGTTC	pBASTA-35S-3FLAG
PBL19-BamH1-R	GGCCGGATCCTCCTCTGACACTAACCCCT	pBASTA-35S-3FLAG
ADR1-KpnI-F	GCGCGGTACCATGGCTTCGTTCATAGATC	pBASTA-35S-3FLAG
ADR1-SalI-R	CGCGTCGACTAATCGTCAAGCCAATCC	pBASTA-35S-3FLAG
EDS1-KpnI-F	CGGGGTACCATGGCGTTTGAAGCTCTTAC	Pcambia1305-FLAG-ZZ
EDS1-XbaI-R	CCGCCGTCTAGAGGTATCTGTTATTTCATCCATC	Pcambia1305-FLAG-ZZ
PAD4-KpnI-F	CGGGGTACCATGGACGATTGTCGATTCGAG	Pcambia1305-FLAG-ZZ
PAD4-BamHI-R	CGCGGATCCAGTCTCCATTGCGTCACTCTC	Pcambia1305-FLAG-ZZ